UCRL 3783

UNIVERSITY OF CALIFORNIA

Radiation Laboratory

TWO-WEEK LOAN COPY

This is a Library Circulating Copy which may be borrowed for two weeks. For a personal retention copy, call Tech. Info. Division, Ext. 5545

BERKELEY, CALIFORNIA

DISCLAIMER

This document was prepared as an account of work sponsored by the United States Government. While this document is believed to contain correct information, neither the United States Government nor any agency thereof, nor the Regents of the University of California, nor any of their employees, makes any warranty, express or implied, or assumes any legal responsibility for the accuracy, completeness, or usefulness of any information, apparatus, product, or process disclosed, or represents that its use would not infringe privately owned rights. Reference herein to any specific commercial product, process, or service by its trade name, trademark, manufacturer, or otherwise, does not necessarily constitute or imply its endorsement, recommendation, or favoring by the United States Government or any agency thereof, or the Regents of the University of California. The views and opinions of authors expressed herein do not necessarily state or reflect those of the United States Government or any agency thereof or the Regents of the University of California.

UCRL-3783

UNIVERSITY OF CALIFORNIA

Radiation Laboratory
Berkeley, California

Contract No. W-7405-eng-48

A STUDY OF THE INTERACTION OF POSITIVE K MESONS

Joseph Edward Lannutti

(Thesis)

May 15, 1957

Printed for the U. S. Atomic Energy Commission

A STUDY OF THE INTERACTION OF POSITIVE K MESONS

Table of Contents

Abstract 4

I. Introduction 5

II. Exposures and Measurements

A. Phase I

1. Exposure System 11

2. Scanning and Measurements 13

B. Phase II

1. Exposure System 15

2. Scanning and Measurements 21

C. Classification of Events 23

III. Conservation of Strangeness 27

IV. K-Hydrogen Cross Section 28

V. Inelastic Interaction Cross Sections

A. The Energy Dependence 33

B. Average K-Nucleon Cross Section 36

C. Charge Exchange and K-Neutron Cross Sections . . 40

D. Angular Distribution of Inelastic Scatters . . . 42

VI. Differential Elastic Cross Section 46

A. 40 to 100 Mev 48

B. 100 to 220 Mev 52

VII. Total Cross Sections 56

VIII. Energy Loss Behaviour 58

IX. Nuclear Excitation 64

X. Scattering Amplitude Analysis 68

XI. Acknowledgments 76

Appendix

A. Phase I Publications . . . . . .

B. Emulsion Composition . . . . . .

C. Phase I Data . . . . . .

D. Phase II Data . . . . . .

E. Calculation of Cross Section per Nucleon . . . .

F. Abstracts of Related Publications . . . . .

Bibliography . . . . . .

A STUDY OF THE INTERACTION OF POSITIVE K MESONS

Joseph Edward Lannutti

Radiation Laboratory
University of California
Berkeley, California

May 15, 1957

ABSTRACT

The interaction of positive K mesons having energies between 20 to 220 Mev with the nuclei of photographic emulsion has been investigated. In this work 237 meters of K meson track were followed and 282 inelastic scatters found. An additional 61 meters of track were followed to search for more K-hydrogen scatters. A total of 15 K-hydrogen events were found.

No case was found in which the K meson lost its rest mass energy in an inelastic interaction. This result supports the concept of conservation of strangeness in fast interactions.

Adding the observed K-hydrogen scatters to the 28 events found by other laboratories at energies above 20 Mev, the K-P cross section is found to be 14.9 $\pm$ 2.3 mb for energies between 20 to 200 Mev. The energy dependence and angular distribution of the K-P scatters are consistent with S wave scattering. The inelastic scattering cross section increases with energy. However, the average K-nucleon cross section is shown to be practically constant at 11 mb for energies from 20 to 180 Mev. The charge exchange cross section is somewhat energy dependent and varies from $2.9 \pm {}^{1.4}_{1.0}$ mb at 70 Mev to 4.0 $\pm$ 0.9 mb at 150 Mev. The angular distribution of the inelastic scatters, assuming that they are scatters from single nucleons in the nucleus, peaks backward in the center of mass system. This effect

is very pronounced above 100 Mev and is probably due to direct neutron scattering since the K-hydrogen scatters appear to be isotropic.

Preliminary results on the analysis of the differential elastic scattering cross sections indicate best agreement with a repulsive potential of about 10 Mev for energies below 100 Mev. The energy loss behaviour of K mesons in inelastic scatters shows strong agreement with that expected for a repulsive potential. The energy loss-angle correlations support the assumption that the K nucleus interaction can be described in terms of single nucleon scatters. The average energy loss of K mesons agrees with the average nuclear excitation for stars caused by K's having energies between 100 to 220 Mev.

Analysis of the data in terms of scattering amplitudes shows that the S wave scattering is predominantly in the T = 1 state but the T = 0 state is not negligible. P wave scattering is shown to be important in the T = 0 state. It is predicted that the charge exchange angular distribution peaks forward. Preliminary data in this connection agrees.

I. INTRODUCTION

In 1947, Rochester and Butler[1] reported the observation of two cloud chamber events which they interpreted as the decay of a neutral particle and the decay of a charged particle of mass considerably greater than that of the pion. Soon after the perfection of photographic emulsion sensitive to minimum ionizing particles, Brown and co-workers[2] in 1949, discovered and correctly interpreted an event in which a singly charged particle of approximately 900 electron masses decayed at rest into three coplanar charged pions. These discoveries opened a new era in fundamental particle research. So many new particles were subsequently found that it became necessary to classify them phenomenologically.[3] A particle of mass between that of a π meson and a nucleon was called a K meson, while one with a mass between that of a nucleon and a deuteron was called a hyperon. The K mesons were further classified according to their decay products as follows:[4]

$$\tau^+ \rightarrow \pi^+ + \pi^+ + \pi^-$$
$$\tau'^+ \rightarrow \pi^+ + \pi^0 + \pi^0$$
$$K^+_{\pi 2} \rightarrow \pi^+ + \pi^0$$
$$K^+_{\mu 2} \rightarrow \mu^+ + \nu$$
$$K^+_{\mu 3} \rightarrow \mu^+ + \pi^0 + \nu$$
$$K^+_{e3} \rightarrow e^+ + (?) + (?)$$
$$\theta^0 = K^0 \rightarrow \pi^+ + \pi^-$$
$$\rightarrow \pi^0 + \pi^0$$

By charge symmetry, decay modes are expected to be similar for K^- mesons and some have been observed.[5]

Hyperons of three mass groups have been found. The approximate masses in electron mass units and the decay modes are as follows:

Hyperon	Mass
$\Lambda^0 \rightarrow p + \pi^-$	2181
$\rightarrow N + \pi^0$	
$\Sigma^+ \rightarrow p + \pi^0$	2327
$\rightarrow N + \pi^+$	
$\Sigma^0 \rightarrow \Lambda^0 + \gamma$	2298 to 2332
$\Sigma^- \rightarrow N + \pi^-$	2341
$\Xi^- \rightarrow \Lambda^0 + \pi^-$	2582

The problem arose as to whether the variety of K meson decay modes from particles of similar masses was due to a single particle with many different modes of decay or to several particles of about the same mass. Analyses of the angle and energy correlation of the decay products of τ^+ and τ'^+ mesons by the method of Dalitz[6] suggested that there were at least two types of K^+ mesons, differing from each other by either spin or parity or both. There analyses suggested that the τ^+ meson had a spin of 0 or 2 and odd parity, whereas if the $K^+_{\pi 2}$ meson has an even spin, it must have even parity. Recent investigations[7], given impetus by this problem, indicate that it is not necessary to conserve parity in decay processes of this nature. So the above arguments to show that there are at least two types of K^+ mesons are no longer valid. Accurate mass measurements of K^+ mesons[8] have shown that

their masses are the same within about two electron masses for the more abundant modes of decay and that the masses agree within experimental error in all cases. Measurements of the K^- meson mass indicate that it is the same as that found for K^+ mesons within the experimental error of a few electron masses.[9] Lifetime measurements of K^+ mesons indicate that the lifetimes of the various decay modes are the same within the experimental errors.[10-11] A study of the interactions of K mesons of the various decay modes would show further if differences exist among them.

To explain why these new strange particles, i.e., K mesons and hyperons, have a long lifetime ($\sim 10^{-10}$ to 10^{-8} sec) and yet are produced in great abundance in high energy interactions between nucleons, and between pions and nucleons, it has been proposed that they are produced only in association with one another.[12] This idea has become generally accepted because no direct evidence against it has been found and two strange particles are frequently seen to be produced in the same nuclear reaction. From the correlation of particle types produced at the interactions of high energy protons and pions with matter, a scheme has been suggested in which a new quantum number is introduced, S for strangeness .[13] The usefulness of the strangeness concept (and the selection rules associated with it) lies in its ability to correlate qualitatively the main features of the production, interaction, and decay of the K mesons and hyperons, as well as to make successful predictions.

The relation between the charge value ($q/|e|$) of a particle

and the z component of its isotopic spin, T_z, is given by the equation

$$q/|e| = T_z + M/2 + S/2$$

where S is the strangeness number of the particle, and M is its baryon number (M = +1 for nucleons and hyperons, 0 for all lighter particles, and -1 for antinucleons and antihyperons). With these assignments, particles which take part in fast reactions have S numbers as follows:

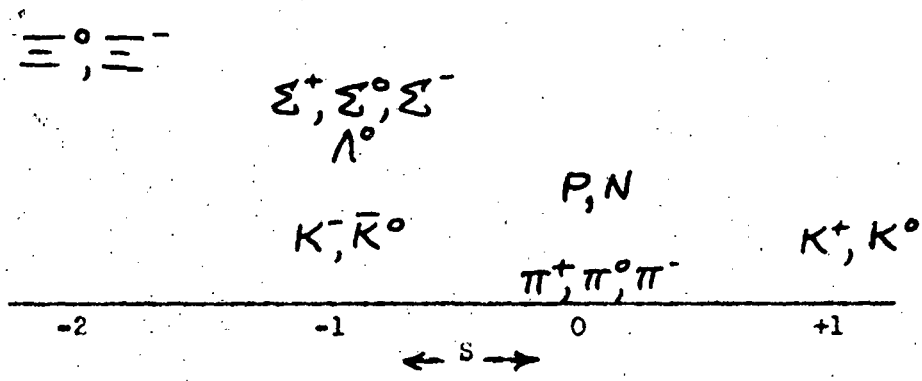

It is proposed that in fast reactions ($\sim 10^{-23}$ sec), such as production of strange particles or their interactions with nuclei, the total S must be conserved. This insures associated production . For slow reactions ($\sim 10^{-10}$ to 10^{-8} sec) such as the decay of particles, the selection rule is $\Delta S = \pm 1$.

K^- mesons are known to go into each of the available channels ($\Lambda^0, \Sigma^+, \Sigma^0, \Sigma^-$) provided,[10,14] and thus conserve strangeness in strong reactions. However, with the known particles, the scheme does not permit the strangeness transfer of a K^+ meson to another particle in a strong reaction. This effect is observed in this experiment.

The work discussed in this thesis has been accomplished during two distinct periods of research. The first part (henceforth called Phase I) was essentially a survey in the sense that it was done early in

the study of K mesons. However, the information gained at that time was of considerable significance since it was the first time that the interaction of positive K mesons with nuclei had been studied. The purpose was an investigation of the properties of a strange particle.

This work supplemented the later work in that it accented energies below 100 Mev. The results of Phase I were published as shown in references 15 and 16.

The second part (henceforth called Phase II) was a more systematic study of K interactions at all energies below 200 Mev with special emphasis on the energy region 100 to 200 Mev. Here the purpose was an investigation of the interaction of a new particle with nuclei.

The exposures and measurements for the two phases will be described separately. The analyses will accent the high energy data as the low energy region has been studied extensively by other groups after our early survey[15,16] (Phase I) was completed and is discussed in the literature.[17,18,19] For convenience, abstracts of these publications are given in Appendix E.

In accomplishing this work, it was deemed desirable to cooperate with other interested physicists at several other laboratories in scanning the stacks so that statistically significant results could be obtained in a shorter period of time. For the work of Phase I, after exposure and development of the stacks, parts of them were sent to A. Pevsner and D. Ritson at the Massachusetts Institute of Technology. The data reported here for Phase I includes that obtained in scanning 12 meters of track at M.I.T. and 24.5 meters at Berkeley. For the work of Phase II, after exposure and development of the stack, a part of it was sent to G. Puppi and G. Quareni at the University of Bologna. The data

reported for Phase II includes that obtained in systematic scanning of 895 meters of track at Bologna and 110.6 meters at Berkeley. In addition 61 meters more were scanned at Berkeley in search for K-hydrogen scatters only. In order that the data might be combined, identical scanning and measurement techniques were used.

II. EXPOSURES AND MEASUREMENTS

A. Phase I

1. Exposure System.

The stacks scanned for Phase I of this experiment were exposed to the K meson beam established at the Bevatron by Kerth and Stork[20]. In these exposures, a copper target in the west tangent tank of the Bevatron was bombarded with 6.2 Bev protons. Particles produced at 90° to the incident proton beam direction were focussed by a magnetic quadrupole system consisting of four quadrupoles with an aperture of 2 inches. The particles then passed through an analysing magnet (with appropriate shielding) which selected particles of a given momentum and cut down extraneous background tracks. Stacks of Ilford G-5 nuclear emulsion were placed at the focus of the particle beam. The total distance of travel from the target to the stacks was of the order of 14 feet. The stacks were oriented so that the particle tracks were parallel to the emulsion layers and were in the direction of the long dimension of the stack. See Figure 1 for a diagram of the experimental arrangement.

The exposures were made with two different momentum-acceptance bands, positive particles of 390 to 450 Mev/c and 335 to 360 Mev/c. In such an exposure, the protons, K^+ mesons, and π^+ mesons (all of the same momentum) have different ranges in emulsion, increasing in that order. The protons stop within a few millimeters to a few centimeters of the entrance edge of the plate depending on the momentum accepted. The length of the plates is such that the K^+ mesons come to rest before reaching the far edge of the plate. The range of the π mesons is so great that they leave the far end of the stack. The π's have a near minimum

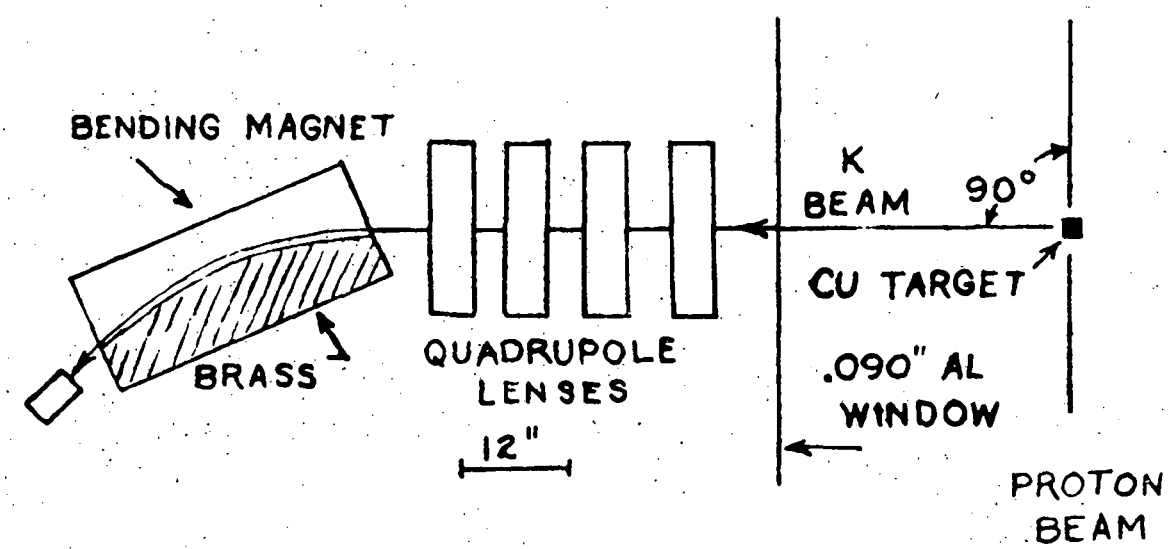

Figure 1

Exposure System for Phase 1

grain density and traverse the stack with very little change and therefore are useful for calibration purposes. It is found in these exposures that the ratio of π mesons to K mesons in the beam is of the order of 100 to 1.

2. Scanning and measurements.

The development procedure used was a modified form of the low temperature method used by emulsion workers at Bristol, England.[21]

The scanning procedure used was as follows: The plates were inspected with high-resolution microscopes by an "along the track" scanning technique. In the region of the plate just beyond where the protons come to rest, tracks are chosen on the basis of grain density. For the momenta accepted, K meson tracks have about twice the minimum grain density. Tracks between 1.8 and 3 times minimum grain density are chosen and followed through the stack. Following from one plate to another is facilitated by a millimeter grid system, with numbers, contact-printed on the bottom side of each emulsion plate.[22] Nearly all tracks selected in this way turn out to be K mesons except for a contamination of about 15% caused by stray protons, π mesons scattered into the stack, and prongs of stars formed in the emulsion.

While following tracks, all scatters with a projected angle greater than 20° were measured and recorded. If the K decayed in flight, it was established as such by grain counts before and after the event and by a multiple-scattering vs. grain count mass measurement before decay. The argument that these were not interactions was based on the fact that in no case had a minimum particle been seen to come from a K^+ interaction which also had one or more evaporation prongs. If the particle being followed had an inelastic interaction and formed a star, all prongs were

followed to rest and identified. If none of the prongs was the K meson or if one of the prongs which might have been the K meson left the stack, the mass of the incoming particle was ascertained by a measurement of multiple coulomb scattering vs. grain count.[23] If the primary was proven to be a K meson and no decay product was seen at the end of any of the prongs even after very careful examination, a mass measurement was made of each prong by using either grain count vs. range, multiple scattering vs. range (constant sagitta method), or opacity vs. range[24]. In cases of doubt, several types of measurement were used. Prongs which left the stack were usually identified by grain density change over the range available. When the K was not found among the visible prongs the interaction was classified as a charge exchange. The non-interacting K's were followed until they came to rest and the decay product found.

Interactions and path length for the K range from 30 Mev to rest were not included. This was necessary to avoid that energy region where analysis of events is extremely difficult since coulomb scattering is predominant and the grain density of the track has saturated.

The energies of the incoming K's for all interactions were established by knowing the mean range of the K's in that region of the plate. The range distribution was determined by the momentum spread which in most of these exposures was of the order of 5%.

The resulting data is given in Appendix B.

B. Phase II

1. Exposure System.

Upon deciding to investigate the interactions of K mesons at a higher energy, it became evident that an attempt to improve the existing K beam systems was desirable. As described previously, in the early exposures the K's were distinguished from the π's which comprised the major part of the beam ($\pi/K \approx 100$) by the fact that the K's had a grain density about twice minimum. At higher energies, however, the grain density of the K's decreases, hence visual recognition of the K's among the π's becomes more difficult. In order to increase the number of K's available for study in a particular stack it would be necessary to expose for a longer time. However, the rather intense integrated flux of π's in previous exposures, because of their large interaction cross section, caused a background of protons confusable with K's of about 15%. In addition the analysis of some events becomes difficult when it must be done in a forest of π meson tracks.

Separation of π's from K's seemed to be the obvious answer to these problems. The simplest scheme was to use a double focussing magnet system with an energy degrader between the magnets. Such a system was already under study by O. R. Price and D. H. Stork and it was reasonable to cooperate on the problem. Price and Stork were designing a system to obtain K's of about 150 Mev. Since it seemed desirable to investigate energies up to 200 Mev, some design differences were necessary. The final physical set up is shown in Figure 2.

The choice of parameters for the system was determined by compromising a number of requirements. Since the multiple Coulomb

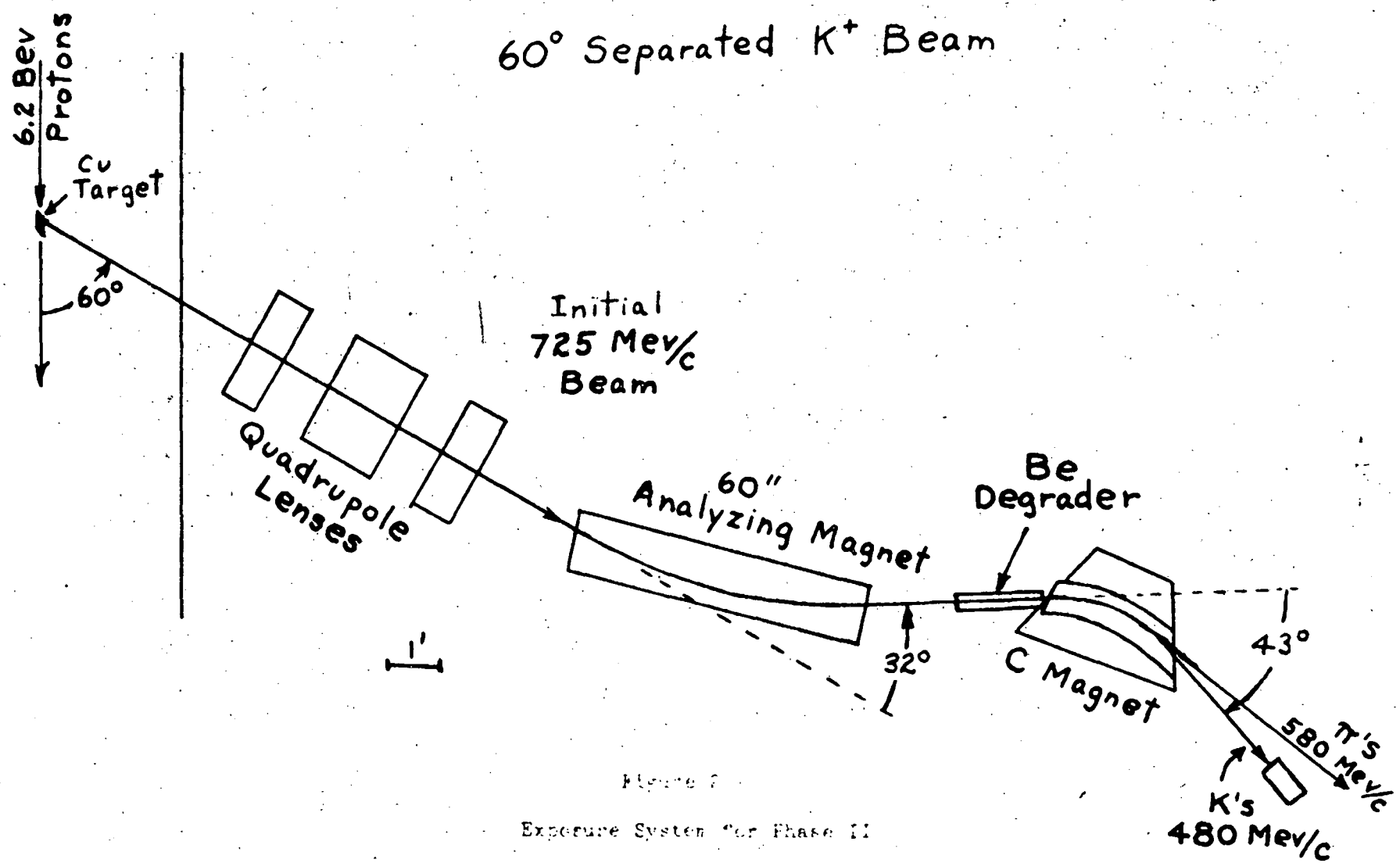

Figure 7

Exposure System for Phase II

scattering would spread the beam after the degrader, the "C" magnet was placed as closely as possible immediately after the degrader to achieve the separation desired before the beam area had become excessively large. The "C" magnet was run at maximum field for maximum separation, with the field direction such as to permit a momentum focus. A maximum momentum spread at the stack position was chosen; this value then determined the momentum bite to be accepted at the slit. The first analyzing magnet was set up for maximum angular deflection, 32°. The slit width and distance from analyzing magnet to slit were determined by the desired momentum bite and by the requirement that the momentum bite accepted be determined primarily by the slit width rather than horizontal image size. Then the spatial beam size for the π's and K's and the π-K spatial separation were studied as a function of degrader thickness.

The choice of accepting particles emitted at approximately 60° was a compromise that enabled high fluxes at a higher momentum and yet allowed facility in setting up beam equipment.

The target mechanism was a drop-string target at the west tangent tank upstream top lock position. The target was copper in the shape of a 60° parallelogram, 1½" long, ½" radially, and 3/8" vertically and a 1/8" by 1/8" by 3/8" polyethylene lip was used.

The optical system parameters (i.e., the quadrupole currents) were worked out originally by Price and Stork for their system of 525 Mev/c initial momentum.[25] Their values were scaled to the desired momenta of 725 Mev/c for this exposure by using the Magnet Testing Group's magnetization curve for an 8" quadrupole.[26] All currents were checked and adjusted before the run by making wire trajectory measurements to locate focal

points and orbits in conjunction with the rest of the system. It had been found that in order to maximize the total flux through the system the first quadrupole was to be turned off, the second to converge vertically, and the third to converge horizontally. The quadrupoles used had 4 inch apertures.

The 60" analyzing magnet currents were set by wire trajectory measurements to give a deflection of 32° for particles of 725 Mev/c. In addition, at the beginning of the run, test plates diagonally imbedded in aluminum were exposed at the slit position with the analyzing magnet set for the required momentum. The distribution of protons in the test plates was found and the momentum of the protons determined from the range in aluminum.

The choice of degrader and its dimensions were established as follows. The primary consideration was the momentum desired at the stack. Since it was considered necessary to stop the K's, the range in emulsion of the upper momentum limit had to be less than 7", the length of the stack to be used. With the previously chosen momentum bite the momentum at the stack was 480 $\pm$ 30 Mev/c. In order to reduce the π/K ratio by a large factor ($\sim$1/100) it was necessary to move the central π momentum about 6" away at the stack position. With the "C" magnet operating at maximum field it was found that the π's had to have a momentum of about 580 Mev/c. In order to get this separation in momenta of the π's and K's through energy loss in a degrader, it was found that an initial momentum of 725 Mev/c and a beryllium absorber of 18.5" (87.0 gms/cm^2) were necessary. Of course, these parameters are all inter-related and the final values were obtained after successive approximations and a knowledge of what beryllium blocks were readily available. The predicted rms spread at the stack due to radial

multiple coulomb scattering was 2.6". The slit system consisted of Be blocks with smallest dimensions 2" in width and 2-3/4" in height, 18.5" total length, and surrounded by copper slabs. All other free volume in the immediate neighborhood was filled with lead. The momentum chosen by the slit was 725 $\pm$ 23 Mev/c.

The "C" magnet had been equipped with a pole-tip shim flared step-wise from entrance, $3\frac{1}{2}$", to exit, 6". This was to increase the field near the degrader where the multiple coulomb scattering spread was still small. The deflection of the K's through the "C" magnet was 43°.

The orbits for the π's and K's in the stack region were found by wire trajectories and the distribution of the π's was measured by test plates and a triple coincidence counter telescope which was swept through the region.

The distance from the target to the degrader midpoint was 17.2 feet and the total distance to the stack was 24.3 feet. The total time of flight for the K's from the target to rest was 1.9×10^{-8} sec. or about 1.4 mean lives.

A few other features of note concerning the system are as follows: (1) As one would expect, at a given angle in the laboratory, the π production decreases with increasing momentum. This behaviour has been observed during the investigations of beam positions for this system and that of Price and Stork. Using the counter telescope it was found that in the region of 400 to 600 Mev/c the π flux varied roughly as $1/p^{3.3}$. (2) L. Stevenson has made a number of phase space calculations (neglecting Fermi motion in the nucleus and any energy dependence of the

matrix elements) to predict the production cross sections of K mesons, produced by a 6.2 Bev beam of protons, at various angles.[27] The initial momentum chosen for this exposure, 725 Mev/c, falls near the peak of the production spectrum for 60° in the laboratory.

The exposure was carried out for 4.7×10^{13} protons on the target. The exposure length was estimated from test plates exposed during the run.

The subsequent study of the stack revealed additional information concerning the exposure:

From the range of the K's in emulsion the energy actually attained was determined to be 180 ± 21 Mev with an almost uniform distribution of K's in that interval. The lower than design value was probably due to a poor determination of current setting for the analysing magnet. The lower central momentum resulted in a shift of the beam to one side of about 1.5", but the size of the image (~ 2") and multiple scattering spread resulted in an average intensity of 250 K's/cm^2 across the stack. Using these numbers and integrating over the expected beam size, it is estimated that the system gave about 13 K's/10^{10} protons on the target over an area of about 250 cm^2.

The flux of lightly ionising particles striking the emulsions was composed of π's, μ's, and electrons. There was one lightly ionising track per K meson in the center of the beam and they increased by a factor of about three on the side of the stack nearest the separated π beam. No serious attempt to identify these particles was made. However, in the process of establishing the minimum grain density for the stack, forty of these tracks were grain counted for 1000

grains as they entered the stack. Roughly, 60% had a grain density of 1.1 x minimum. This indicates that this proportion could have been high energy electrons.

The background of protons having the same grain density as the K's was about 2%. These were easily eliminated by making a second grain count as the track left the stack and comparing with expected grain density variation with range.

2. Scanning and measurements.

The scanning procedure was very similar to that discussed for Phase I of this experiment, with the exceptions discussed below:

The K tracks again were distinguished by grain density. The K's had grain densities ranging from 1.5 to 1.9 times minimum. Tracks were found 5 mm from the entrance edge. In this exposure the energy spread was about 21 Mev. Therefore, in order to determine the energy distribution and to have a reference for the energy of the K's at interactions, it was necessary to make a good grain density determination (to 5%) of each track as it was found. This initial energy determination, calibrated against those tracks which came to rest, enabled one to know at what energy the K interacted, decayed in flight, left the stack or scattered before leaving the stack.

In order to study the elastic differential cross section for interference phenomena, during this part of the experiment all scatters with projected angles of 2° or greater were measured (both projected and dip angles) and recorded. This was done for each track from its beginning to three millimeters from its end (i.e., $T_K > 20$ Mev). By measuring the distance of each scatter to the end of the track, the energy of each

scattering event was also determined.

All inelastic events were analyzed as discussed in Phase I. Special emphasis was placed on attaining the energy loss at each interaction. This was accomplished by a good grain count (500 to 1000 grains) just before each interaction to determine the energy of the incoming K and then subtracting the energy of the outgoing K (determined from its range after scatter or another grain count if it went out of the stack). This energy loss determination was made for all scatters with space angle greater than 40° (i.e., elastic as well as inelastic) and all scatters less than 40° which had prongs or a visible grain density change.

As it was desirable in the second phase of this work to accent the high energy region, two scanning variations were used. At first all K's were grain counted for 500 grains at the entrance to the stack and then followed until they came to rest, recording all information discussed here. About 450 of the K's followed in this fashion came to rest without making any inelastic scatter or elastic scatter greater than 20°. The distribution in range of these K's was used to obtain the distribution in energy of the K meson beam. In subsequent scanning all tracks were followed for a constant distance (45 mm) after being chosen at 5 mm from the edge. This distance was chosen to insure that almost all tracks followed were in the energy region above 100 Mev. The path length distribution in energy for this subsequent scanning was based on the path length distribution in energy of the first 45 mm of the 450 K's followed to rest.

The resulting data is given in Appendix C.

C. Classification of Events

Throughout this work an attempt has been made to classify each event as either elastic, inelastic, or charge exchange. The identification in some cases was ambiguous.

Elastic interactions refer to those cases when the K meson interacted with the nucleus as a whole and energy and momentum were conserved. In colliding with a light nucleus in emulsion this could mean a considerable energy loss but would result in a visible recoil. This type of collision with light nuclei is identified as discussed in Appendix C and is classified as elastic. The energy loss measurement techniques have a limited resolution. The methods used are the change in range among the interacting and non-interacting K's or the grain density before and the range after the interaction. The resolution in each case is about the same, but for this work the latter technique was used extensively since it was applicable throughout the experiment. The resolution then is, to a certain extent, a function of how much grain counting one does. A compromise gave a resolution which varied from 8% to 12% in the energy range 20 Mev to 200 Mev. Therefore a general cut-off of 10% was adopted. This meant that if a measurement of energy loss for a given event indicated it was less than 10% it was classified as elastic. Of course, this classification is not always correct since it is possible to excite low lying rotational levels of the nuclei. Thus a K could lose several Mev in such an inelastic process and still be classified as elastic. Further, and this is more important here, in the high energy interval accented in this work the

resolution is from 10 to 20 Mev. Thus it is possible for the K meson to knock-out or evaporate out one or two neutrons and yet have an energy loss of less than 10% and be classified as elastic. Three events were found which had an energy loss of less than 10% and yet emitted an evaporation type proton. These were included among the inelastic events and were weighted as double in any distribution of events to allow somewhat for similar neutron events. This was actually a small correction among the 282 inelastic events, but points up the fact that the reaction cross sections quoted represent a lower limit. However, it should be mentioned here that the Pauli exclusion principle will prohibit a large fraction of the scatters where the energy loss is less than 10%.

In those cases classed as charge exchanges, considerable effort was expended to ascertain that the K meson was not among the visible prongs. If a prong was longer than three millimeters its identity could be and was established by direct measurement of scattering or ionization properties. If shorter, proof that it was not a K had to be based on the fact that no decay product was seen. This proof was quite good provided the track ended at least 20μ from either surface. With the development used, K decay secondaries have grain densities at least 21 grains/100μ and one experienced with K^+ mesons in emulsion can find secondaries with nearly 100% efficiency if clear of either surface. At the surface the efficiency drops to about 80% since the secondary may go into the next plate and be difficult to locate. In this experiment the several prongs which ended near the surface and were still in doubt were shorter than 1 mm. The 280 other inelastic events contained only one which had a K coming out with a range of 2 mm. The next shortest was 4 mm. On these grounds it was assumed that these dubious prongs were not K mesons.

The classification of an event as a charge exchange rather than absorption of the K meson was based on the small visible energy release which never exceeded the kinetic energy of the incoming K. Table I gives a comparison of various properties of ordinary inelastic events and charge exchange events for the data on K's above 100 Mev. In the compilation of the prongs only those having a length greater than 10μ are considered to avoid the region of delta rays and recoils. The average number of evaporation prongs is larger for the charge exchange events. This is due to the fact that when there is a charge exchange and an appreciable nuclear excitation, the resulting proton excess makes the evaporation of protons more probable. Beta decay of the residual nucleus occurs when the excitation is small.

Another interesting consistency pointed out by this comparison is that in roughly 40% of the charge exchange events a proton appears as a knock-on or cascade proton, presumably the direct product of the interaction $K^+ + N \longrightarrow K^0 + P$. If one assumes that the cross sections for interaction with protons and neutrons are comparable then one would expect that 20% of the ordinary inelastic events would also have knock-on protons and this seems to be true. However, this table includes the data on only 22 charge exchange events. More scanning is presently in progress to increase the data in order to study this effect.

Note also that if one considers only stars with cascade protons, the visible energy in cascade prongs is the same as the average energy loss of the K mesons, indicating that a quasi-elastic scattering took place.

Table I

Comparison of Charge Exchange Events

with Ordinary Inelastic Events

100 to 220 Mev

(Based on Berkeley data only)

	Ordinary Inelastic	Charge Exchange
$\frac{\text{Total No. Visible Prongs } (R > 10u)}{\text{Total No. Stars}}$	0.88	1.20
$\frac{\text{No. of Evaporation Prongs } (10u < R < 1.2 \text{ mm})}{\text{Total No. Stars}}$	0.57	0.96
$\frac{\text{No. of Cascade Prongs } (R > 1.2 \text{ mm})}{\text{Total No. Stars}}$	0.24	0.50
$\frac{\text{Total Visible Energy (Incl. Binding Energy)}}{\text{Total No. Stars}}$	24 Mev	35 Mev
$\frac{\text{Visible Evaporation Energy (Incl. B. E.)}}{\text{Total No. Stars}}$	8.4 Mev	12.2 Mev
$\frac{\text{Visible Cascade Energy (Incl. B. E.)}}{\text{Total No. Stars}}$	15 Mev	25 Mev
$\frac{\text{Visible Cascade Energy (Incl. B. E.)}}{\text{No. Stars with Cascade Prongs}}$	67 Mev	60 Mev
Average Kinetic Energy Loss of K's	67 Mev	-

III. CONSERVATION OF STRANGENESS

One effect of great interest in this work is the fact that so far no positive K meson interaction has been observed in which the K meson gives up its rest mass energy. The limits can be expressed as no case observed in 282 inelastic interactions reported here. This singular effect among the light and heavy mesons supports the scheme presented by Gell-Mann and others[13] for a positive strangeness particle. According to these schemes it is not possible for a K^+ meson to produce any of the known hyperons in a strong reaction because it would require a strangeness change of two which violates the selection rule that $\Delta S = 0$ in strong reactions. However, these schemes do not rule out the possibility that a hyperon of strangeness +1 could be produced. None was found.

In addition, no evidence was found for the production of an excited fragment containing a bound K meson. The metastability and decay of such fragments has been discussed by Pais and Serber.[28]

IV. K-HYDROGEN CROSS SECTION

Among the interactions of K^+ mesons with emulsion nuclei, those with free protons are of special interest in studying K-nucleon forces. As can be seen by the table in Appendix B, 5.3% of the total geometric cross section presented by emulsion nuclei is due to hydrogen. Hence, it is possible to measure the K-hydrogen cross section. These events are distinguished from the other nuclear interactions because the tracks are coplanar and there is momentum and energy conservation.[29]

The determination of the K-P cross section in this manner has been found to be especially difficult due to the extreme rarity of events (a consequence of the apparent small cross section) and the great scanning effort necessary for a statistically significant result. Some events have been found in this experiment and are given in Table II.

The first event of this table found in Phase I was published when found as of special interest at that time since it gave a first good mass measurement of a K meson other than the τ.[30] It gave a mass of 973 $\pm$ 12 electron masses and from grain counts on the decay product is believed to have been a $K_{\pi 2}$.

Data gained on the K-P interactions in the systematic scanning reported herein has been supplemented by a rapid scanning technique to locate K-P scatters above 100 Mev. Other interactions were not analyzed during this scanning.

The events found have been combined with 28 events available from other laboratories doing similar work with emulsion (Gottingen - 14 events, Padova - 6 events, Brookhaven - 4 events, Dublin - 2 events, Rochester - 1 event, and Bristol - 1 event)[31]

and the cross section evaluated in four energy intervals. These results are shown in Figure 3. The statistics are still poor, but this data is consistent with a constant cross section in the interval 20 to 200 Mev. The mean cross section over the total interval becomes 14.9 ± 2.3 mb. Shown also on the plot, for comparison, are the results of the Michigan propane bubble chamber group[32] (9.4 ± 1.7 mb for the interval 20 to 90 Mev) and the counter result of Kerth, et al.[33] (15.4 ± 3.0 mb at 192 ± 25 Mev). The propane bubble chamber result is slightly lower, but this might be due to the experimental bias against small angles if the cross section is isotropic.

The distribution in angle of all the emulsion data is shown in Figure 4. The data is still too meagre for definite conclusions but the distribution is consistent with S-wave scattering. The new data somewhat alters the earlier conclusion discussed in the literature (see Appendix E) that the K-P angular distribution was most compatible with a superposition of Coulomb scattering upon S-wave repulsive nuclear scattering. The sign of the potential is no longer clear. However, the coulomb scattering and interference effect is not as great at the higher energy at which the bulk of the additional data was obtained.

Hence, the available emulsion data at this writing indicates that the K-P interaction is mainly S wave for energies between 20 to 200 Mev.

Table II

K-HYDROGEN SCATTERS

	Event Code	Incident Energy	Laboratory Angle	Center of Mass Angle
Phase I:				
	S1	102 Mev	39°	60°
	SC15	121	20	32
Phase II:				
	F043	69	98	130
	37/7	86	50	75
	6228	91	72	105
	6086	104	94	128
	5075	117	65	95
	5330	118	43	67
	1073	129	99	132
	37/2	138	37	58
	5196	146	77	111
	8087	152	24	39
	6574	165	75	108
	1039	174	76	110
	5210	185	91	127

Figure 3

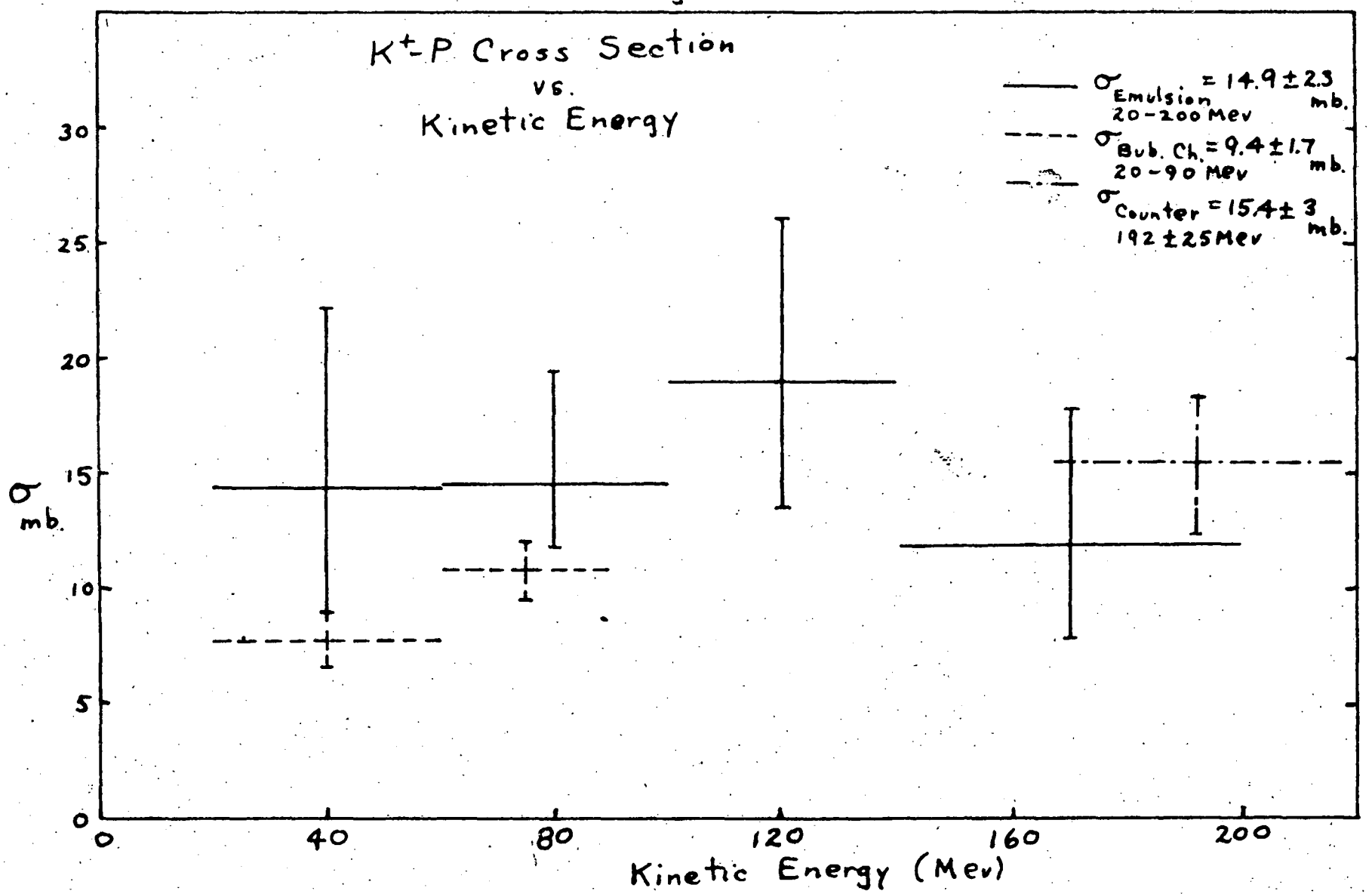
K+-P Cross Section
vs.
Kinetic Energy
σ Emulsion = 14.9 ± 2.3 mb.
20-200 Mev
σ Bub. Ch. = 9.4 ± 1.7 mb.
20-90 Mev
σ Counter = 15.4 ± 3 mb.
192 ± 25 Mev
σ mb.
0
5
10
15
20
25
30
0
40
80
120
160
200
Kinetic Energy (Mev)

Figure 4

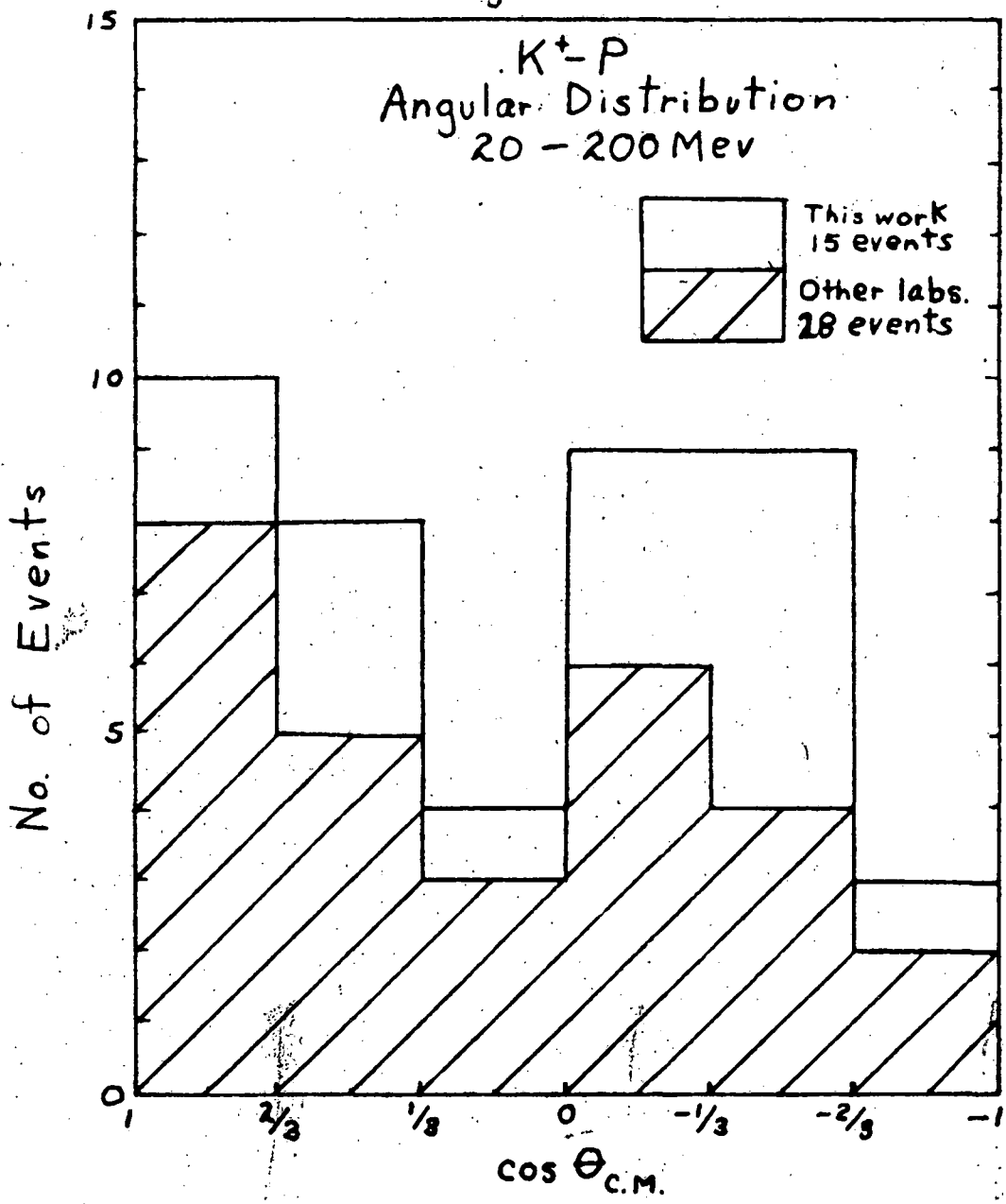
$K^+ - P$
Angular Distribution
20 – 200 Mev
This work
15 events
Other labs.
28 events
No. of Events
15
10
5
0
1
2/3
1/3
0
-1/3
-2/3
-1
cos $\theta_{C.M.}$

V. INELASTIC INTERACTION CROSS SECTIONS

A. The Energy Dependence of the Inelastic Scattering Cross Section.

Figure 5 shows the path length distribution in 10 Mev intervals as well as the distribution of inelastic interactions (i.e., inelastic scatters with prongs or energy loss greater than 10 % and charge exchange scatters). This plot includes all data from Phases I and II of this experiment obtained in the systematic type of along the track scanning. The path length (which is the quantity corresponding to the flux in a counter experiment) studied in each interval is not constant.

The information given in Figure 5 was used to obtain the variation of cross section for inelastic interactions with energy. This has been done in 40 Mev energy intervals and is shown in Figure 6. There is no rapid change apparent below 200 Mev. The rise near 200 Mev based on this data alone is not statistically significant.[34] A steady increase is noted, however, and for the purposes of this report the data has been split into two large energy intervals, 20 to 100 Mev (average energy 70 Mev) and 100 to 220 Mev (average energy 150 Mev). Then, averaging the data in these intervals one obtains

Energy Interval	For Emulsion Mean Free Path	For Emulsion Cross Section
20 - 100 Mev	104^{+14}_{-10} cm.	206 ± 23 mb.
100 - 220 Mev	$75.3^{+5.7}_{-4.8}$ cm.	284 ± 20 mb.

where the cross section calculation excludes hydrogen and hydrogen scatters. The events included are the inelastic scatters and the charge exchange scatters only.

Figure 5

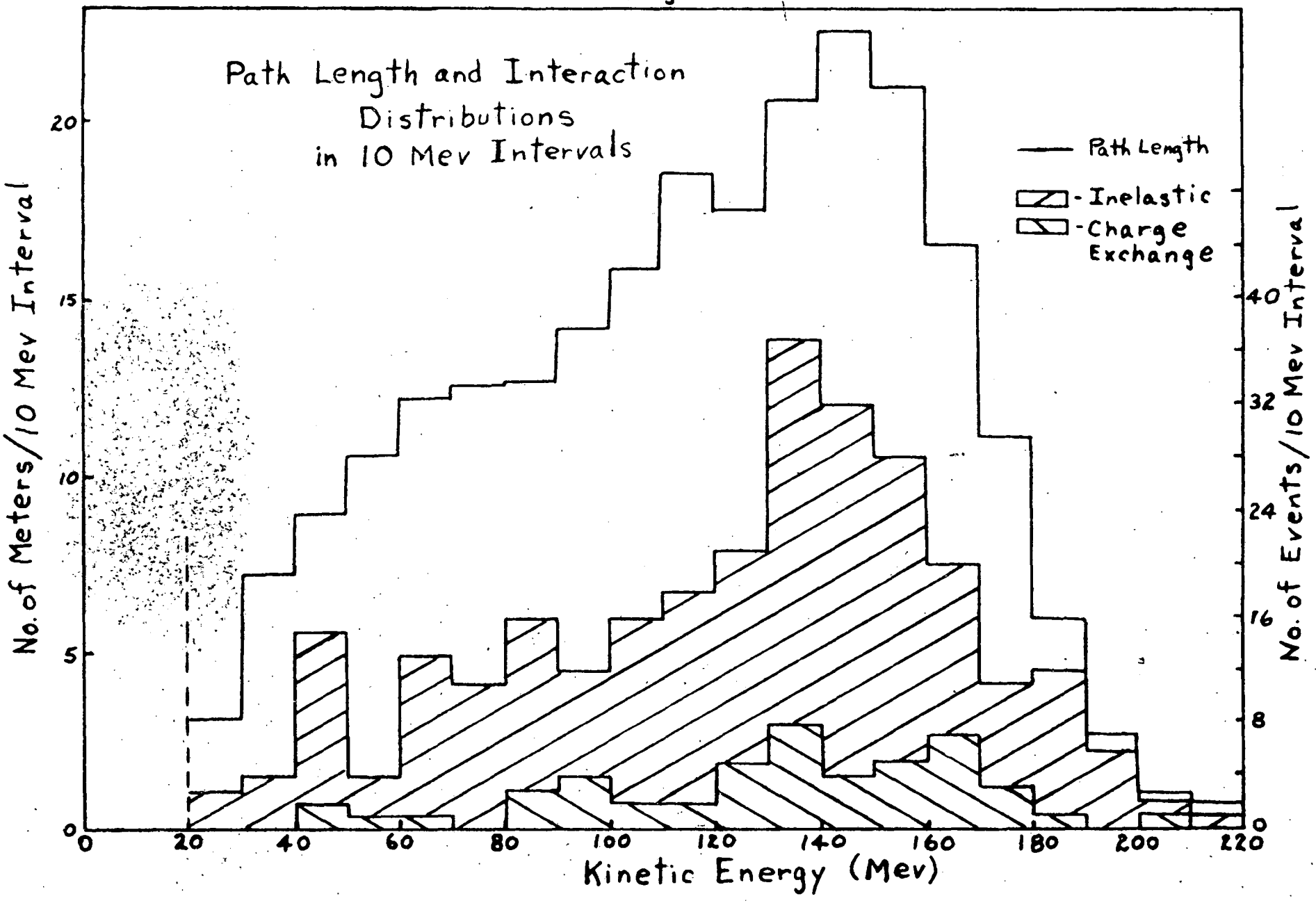
Path Length and Interaction
Distributions
in 10 Mev Intervals
Path Length
- Inelastic
- Charge
Exchange
No. of Meters/10 Mev Interval
No. of Events/10 Mev Interval
Kinetic Energy (Mev)
0
5
10
15
20
0
8
16
24
32
40
0
20
40
60
80
100
120
140
160
180
200
220

Figure 6

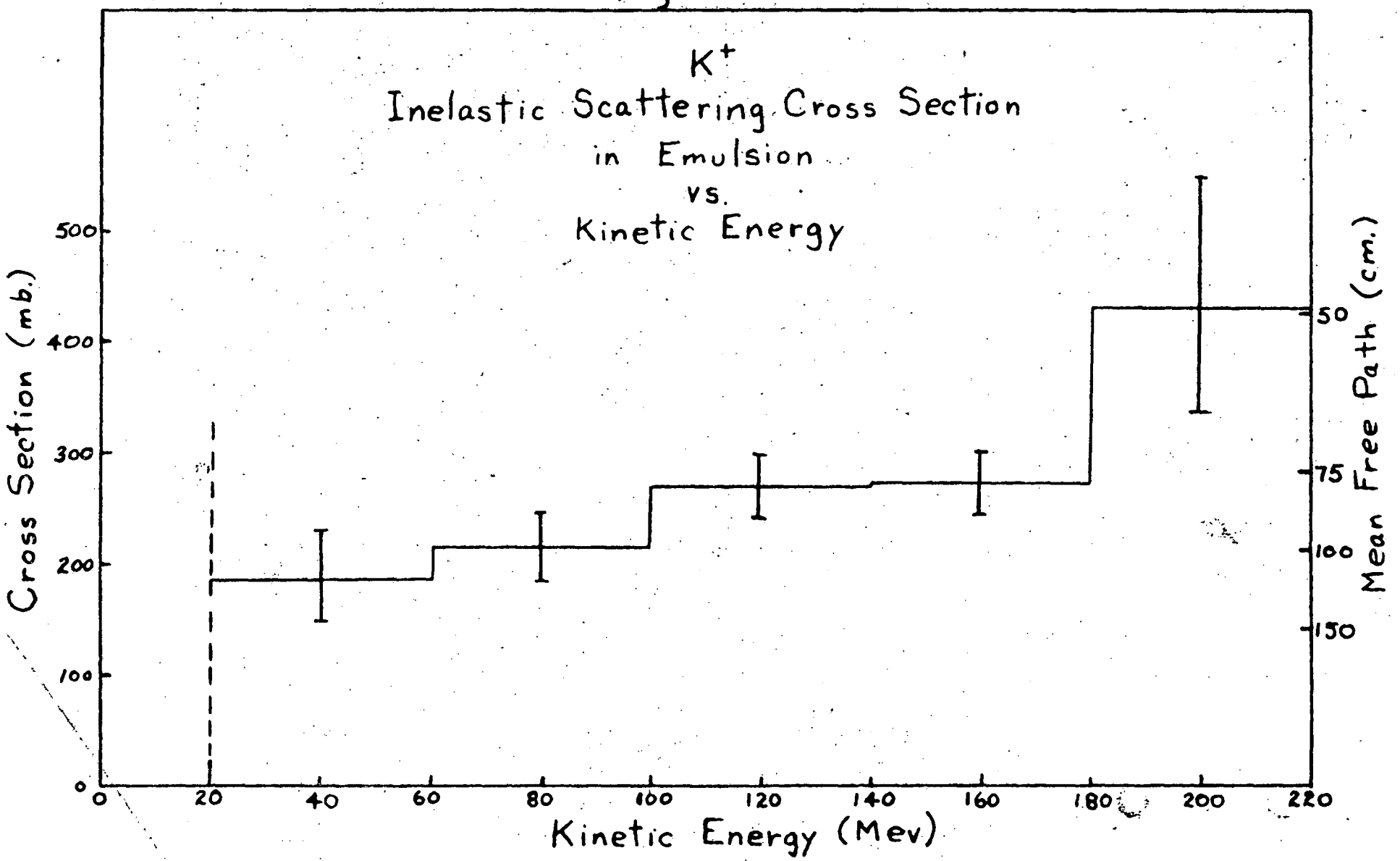
K^+
Inelastic Scattering Cross Section
in Emulsion
vs.
Kinetic Energy
Cross Section (mb.)
0
100
200
300
400
500
Mean Free Path (cm.)
50
75
100
150
0
20
40
60
80
100
120
140
160
180
200
220
Kinetic Energy (Mev)

B. K-Nucleon Cross Section

The inelastic interaction of high energy neutrons with heavy nuclei can be described in terms of a simple model in which the nucleons within the nucleus are assumed to act as independent scattering centers, unaffected by their neighbors[35,36]. The nucleus is considered as a degenerate Fermi-Dirac gas of neutrons and protons without mutual interaction.

This model should be applicable here. The mean deBroglie wavelength for the K's in this experiment is of the order of the nucleon size. The observed mean free path in emulsion for an inelastic interaction is long (2 to 3 times geometric) so that the inelastic cross section must be small. Applying the model it is possible to deduce the cross section for an elementary collision with a single nucleon. The details of the calculation are given in Appendix D.

In this calculation, allowance is made for the decrease in the observed cross section due to Coulomb repulsion. A further correction of similar nature that has been neglected here involves the repulsion experienced by the wave function representing the incident particles in the region of a repulsive real nuclear potential. This could be considered reflection in the limiting case of a square well potential. The effect is small if the magnitude of the real potential is small. At present the nuclear potential is thought to be of the order of 10 Mev for incident K meson energies below 100 Mev but is uncertain at higher energies. This is discussed further in Section VI.

Further correction must be made for the Pauli exclusion principle

which greatly limits the number of small energy transfers to bound nucleons. Accordingly, an interaction that would leave the nucleon in an occupied quantum state is forbidden. Thus the cross section for interaction with a nucleon, $\bar{\sigma}$, within a nucleus will be less than that with a free nucleon by a factor f(T), depending on the K meson energy, T. For interactions with an "average" bound nucleon then

$$\bar{\sigma} = f(T)\,\frac{Z\sigma_{KP} + (A-Z)\,\sigma_{KN}}{A} \qquad \text{(B-1)}$$

where σ_{KP} and σ_{KN} are the cross sections on a free proton and neutron, respectively. Treating the nucleons within the nucleus as forming a degenerate Fermi-Dirac gas with a maximum Fermi energy of 25 Mev, and following the analysis of Goldberger[36], the factor has been calculated by R. M. Sternheimer[37] for various incident K meson energies. The neutron and proton differential cross sections were assumed to be isotropic. His results were used to correct the cross sections for the exclusion principle reduction.

These calculations have been made for the five energy intervals shown in Figure 6 and are given in Table III. To indicate the effects of the various corrections, the uncorrected value of the average nucleon cross section is given and then the corrections are applied. $\bar{\sigma}_1$ is the cross section obtained if calculated with the assumption that there is no shading and emulsion is just a sea of nucleons, $\bar{\sigma}_2$ is the result obtained correcting for nucleon shading as described in Appendix D. $\bar{\sigma}_3$ is the result when Coulomb repulsion effects are also considered as described in

Appendix D. $\overline{\sigma_4}$ is the result using the incident K meson energy to estimate the reduction due to the Pauli exclusion principle. $\overline{\sigma_5}$ is the result if one assumes that the incident K meson energy is reduced by 20 Mev before interaction to allow for the repulsive Coulomb and repulsive nuclear potential.

The large cross section in the last energy interval based on this data alone is not statistically significant.[34]

The data has been divided into two large energy intervals and the average cross section per nucleon calculated with corrections similar to those of Table III. The results are

Energy Interval	Average Energy	$\overline{\sigma_3}$ (mb)	$\overline{\sigma_5}$ (mb)
20 - 100 Mev	70 Mev	$6.6^{+1.5}_{-1.0}$	$10.8^{+2.5}_{-1.6}$
100 - 220 Mev	150 Mev	$9.6^{+1.3}_{-1.1}$	$11.3^{+1.8}_{-1.5}$

It appears that the cross section per nucleon calculated in this fashion is constant in the region studied at about 11 mb.

TABLE III

T (Mev)	M.F.P. (cm.)	σ_{em} (mb)	$\bar{\sigma}_1$ (mb)	$\bar{\sigma}_2$ (mb)	$\bar{\sigma}_3$ (mb)	$\bar{\sigma}_4$ (mb)	$\bar{\sigma}_5$ (mb)
20 - 60	115^{+28}_{-22}	186^{+44}_{-36}	$3.7^{+0.9}_{-0.7}$	$4.9^{+1.6}_{-1.2}$	$6.4^{+3.3}_{-1.4}$	$11.6^{+6.0}_{-2.5}$	$21.4^{+11.0}_{-4.7}$
60 - 100	99^{+16}_{-12}	216 ± 30	4.5 ± 1.4	$5.9^{+1.2}_{-1.0}$	$8.8^{+1.4}_{-1.2}$	$8.9^{+1.8}_{-1.6}$	$10.1^{+2.1}_{-1.8}$
100 - 140	79^{+9}_{-8}	271 ± 28	5.7 ± 0.6	$8.1^{+1.3}_{-1.1}$	$9.1^{+1.8}_{-1.4}$	$11.0^{+2.2}_{-1.7}$	$11.1^{+2.2}_{-1.7}$
140 - 180	78^{+9}_{-7}	274 ± 29	5.7 ± 0.6	$8.2^{+1.3}_{-1.1}$	$9.0^{+1.6}_{-1.4}$	$10.2^{+1.8}_{-1.6}$	$10.5^{+2.1}_{-1.8}$
180 - 220	49^{+15}_{-11}	433^{+116}_{-94}	$9.1^{+2.5}_{-2.0}$	$\sim 17 \pm 6$	$\sim 18 \pm 6$	$\sim 20 \pm 7$	$\sim 20 \pm 7$

T is the incident kinetic energy of the K meson. M.F.P. is the mean free path for inelastic interaction in emulsion. σ_{em} is the cross section calculated from the mean free path in emulsion (excludes hydrogen). $\bar{\sigma}_1$ is the cross section per nucleon obtained if calculated with the assumption that there is no shading of nucleons. $\bar{\sigma}_2$ is the result obtained accounting for nucleon shading. $\bar{\sigma}_3$ is the result with allowance for Coulomb repulsion. $\bar{\sigma}_4$ is the result with exclusion principle correction using the incident energy of the K. $\bar{\sigma}_5$ is the result with exclusion principle correction using the incident energy reduced by 20 Mev. A nuclear radius $r_0 A^{1/3}$ with $r_0 = 1.2$ Fermis has been used.

C. Charge Exchange and K-neutron Cross Sections

Charge exchange events are unique among the inelastic interactions as there is no doubt that they were interactions with neutrons. With the assumption that the K nucleus interactions are scatters with single nucleons in the nucleus, it is possible to estimate the charge exchange cross section per neutron.

It is found that a certain fraction, f, of the inelastic interactions are charge exchange scatters. Defining $\sigma_{KN} = \sigma_{N+} + \sigma_{No}$ where σ_{N+} represents the cross section for direct scattering from neutrons and σ_{No} is the cross section for charge exchange scattering, then

$$\bar{\sigma} = \frac{Z\sigma_{KP} + (A-Z)(\sigma_{N+} + \sigma_{No})}{A} \qquad (C-1)$$

It follows that the fraction, f, gives σ_{No} since

$$(A-Z)\sigma_{No} = f\left[Z\sigma_{KP} + (A-Z)(\sigma_{N+} + \sigma_{No})\right] = fA\bar{\sigma}$$

so

$$\sigma_{No} = f\left(\frac{A}{A-Z}\right)_{Ave.}\bar{\sigma} \qquad (C-2)$$

Using $(A/A-Z)_{average}$ as 1.84 and the observed values of f for the two energy intervals:

Energy Interval	f	Charge Exchange Cross Section
20 - 100 Mev	$0.14\ ^{+0.06}_{-0.04}$	$2.9\ ^{+1.4}_{-1.0}$ mb
100 - 220 Mev	0.19 ± 0.03	4.0 ± 0.9 mb

where the $\bar{\sigma}_b$ values of the previous section have been used.

There may be a slight increase in the charge exchange cross section with increasing energy, but the data of this experiment alone is insufficient to prove the effect conclusively.[38] In this connection, the following table gives the ratio of the number of charge exchange events to the number of non-charge exchange inelastic events in five energy intervals.

Energy Interval	C.E./Non-C.E.
20 - 60 Mev	3/23 = 0.13
60 - 100 Mev	8/44 = 0.18
100 - 140 Mev	17/75 = 0.23
140 - 180 Mev	19/72 = 0.26
180 - 220 Mev	3/18 = 0.17

Using equation C-1 and the K-P cross section for free protons (see Section IV) the cross section for direct K-neutron scattering has also been estimated.

Energy Interval	K-neutron cross section
20 - 100 Mev	4.7 ± 4.7 mb
100 - 220 Mev	$3.6 \,^{+4.8}_{-3.6}$ mb.

D. Angular Distribution of Inelastic Scatters

Figure 7 gives the angular distributions of inelastic scatters in the laboratory system in two energy intervals. It appears that within the statistics of the data the distribution is nearly isotropic except for some forward peaking. These distributions have to be interpreted as a complex effect resulting from elementary scattering due to a K-nucleon cross section of still unknown shape in the center of mass system corrected by the action of the Pauli principle in nuclear matter plus the effect of the nucleon repulsive potential.

As a first approximation, the refraction effect of the nuclear potential in changing the angles of the K entering and leaving the nucleus is neglected. The nuclear potential will then be effective only in diminishing the energy of the K on entering the nucleus. Owing to the small total nucleon cross section, the probability that the same K makes two successive collisions is small, so that practically all inelastic events may be supposed to be due to a single collision, and the observed angle will be the true scattering angle in the laboratory system.

With these assumptions it is possible to convert the laboratory angles to angles in the center of mass system, taking into account the Fermi motion of the nucleons. The conversion cannot be made exactly because the motion of the nucleon struck is not known. However, an approximation to the correct distribution in the center of mass can be obtained by considering each scatter as though it were on a nucleon at rest. This has been done for each scatter and the results are plotted in Figure 8.

Figure 7(a)

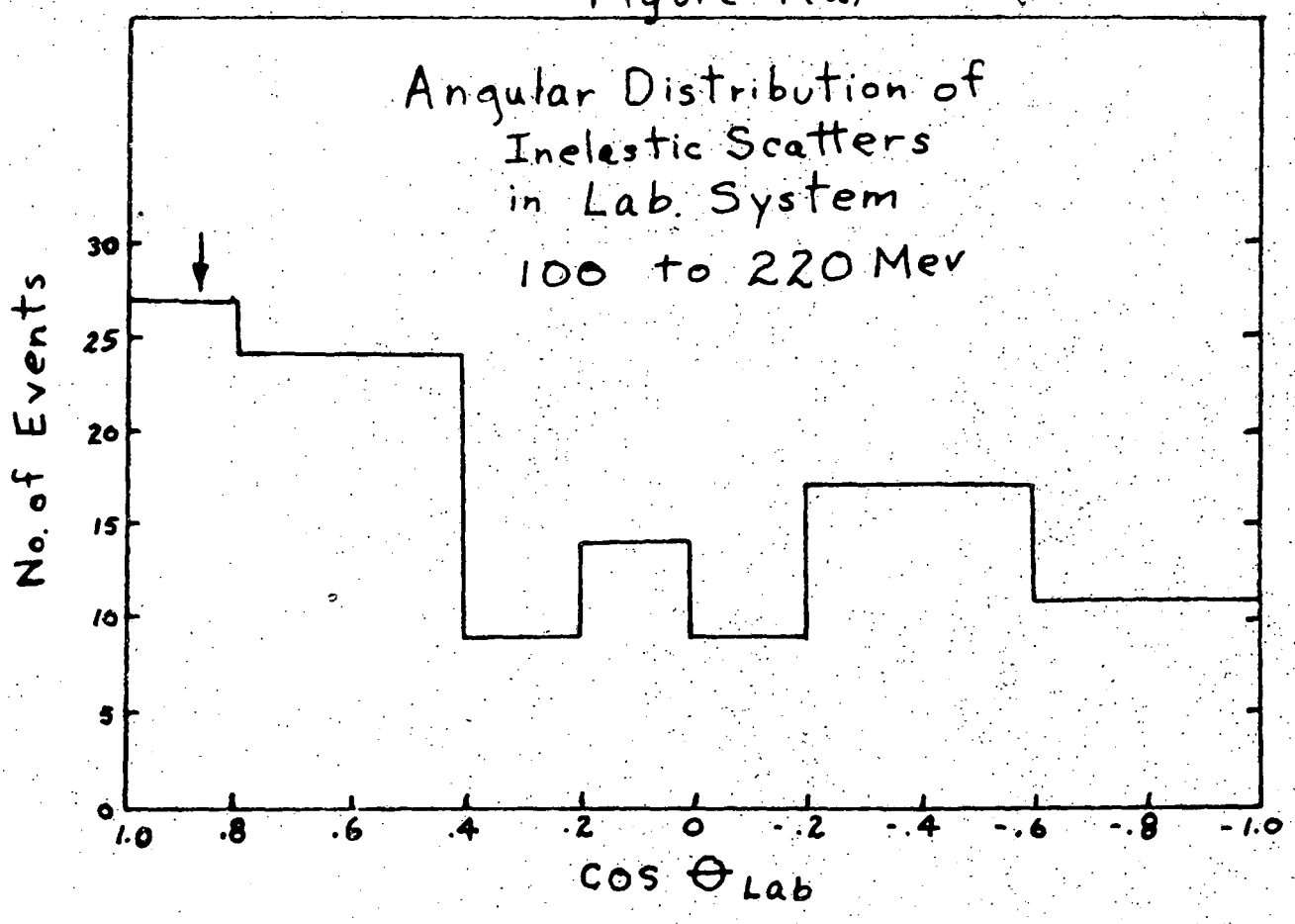

Figure 7(b)

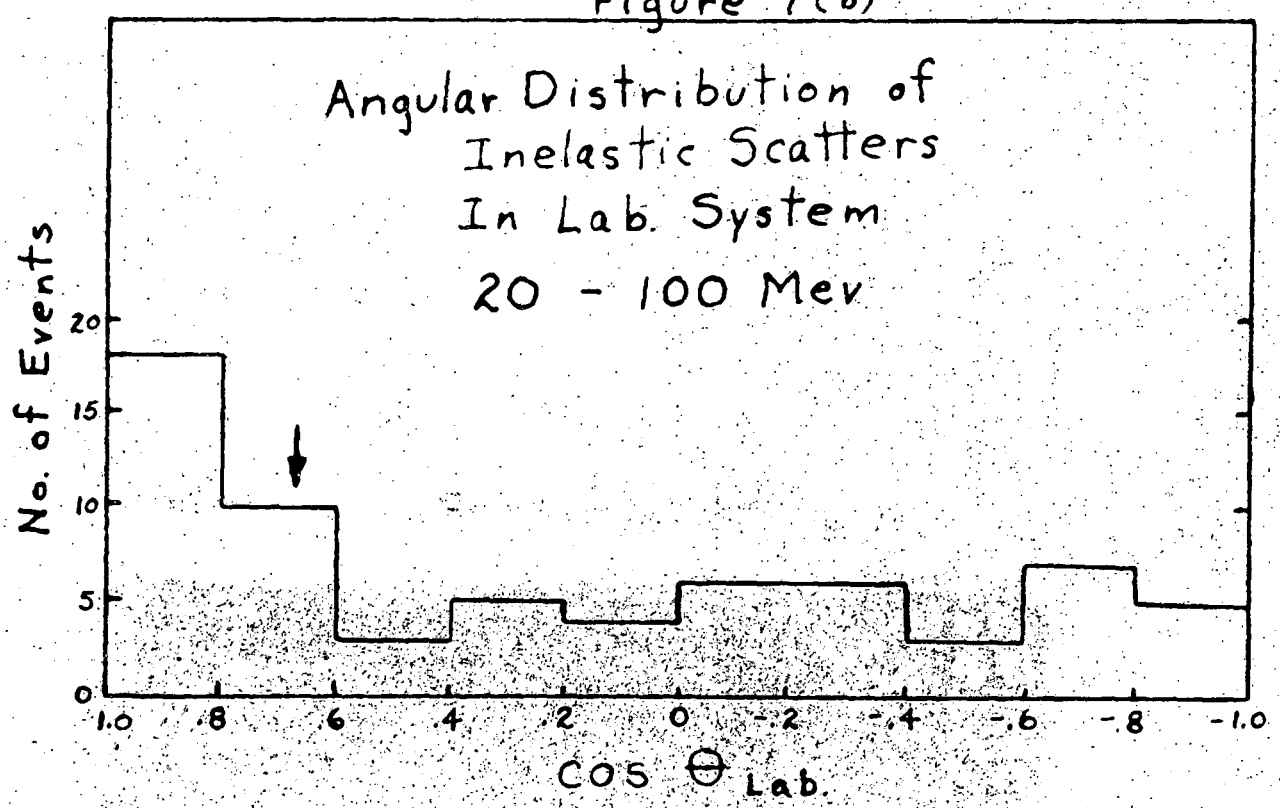

Figure 8 (a)

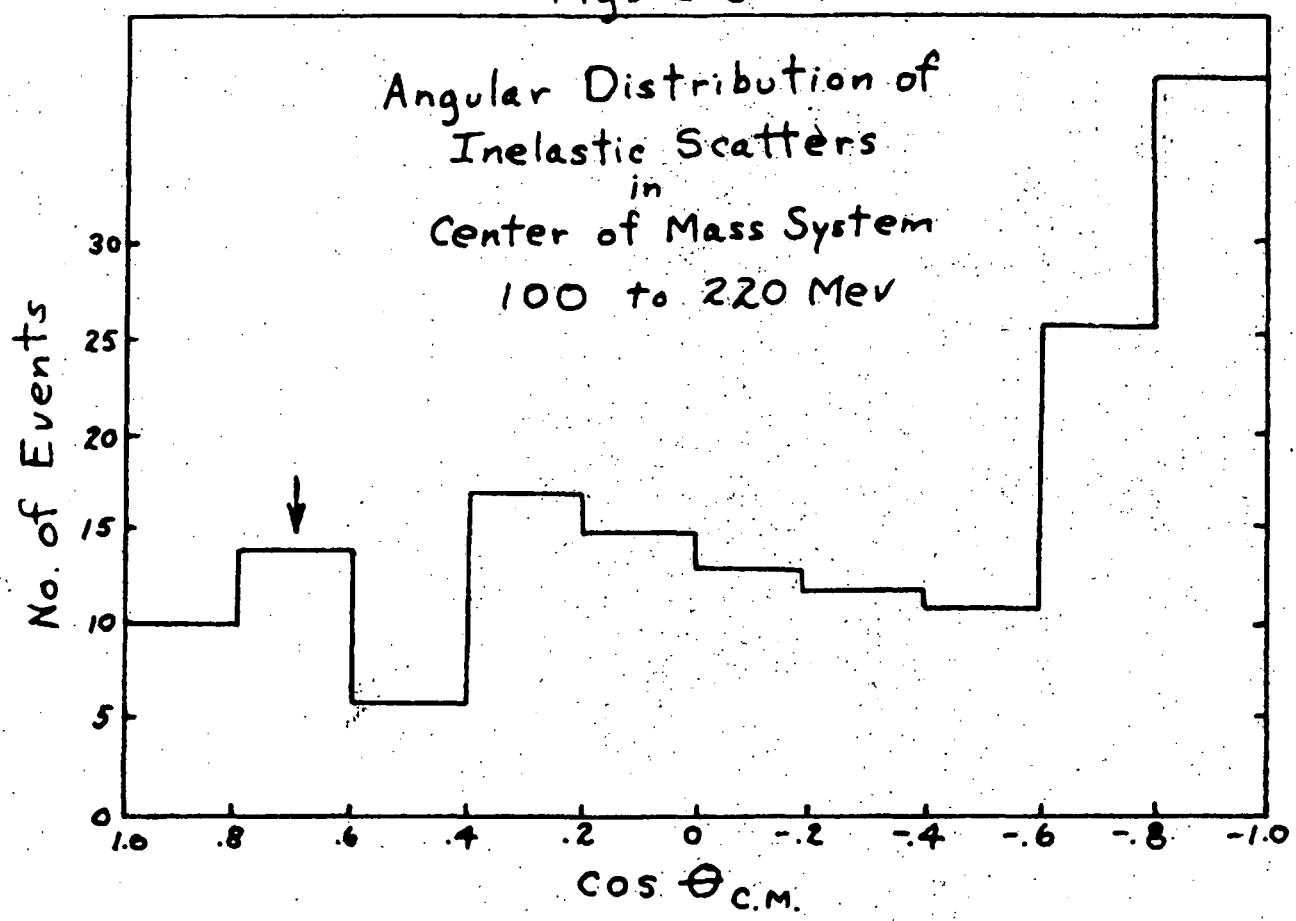

Figure 8 (b)

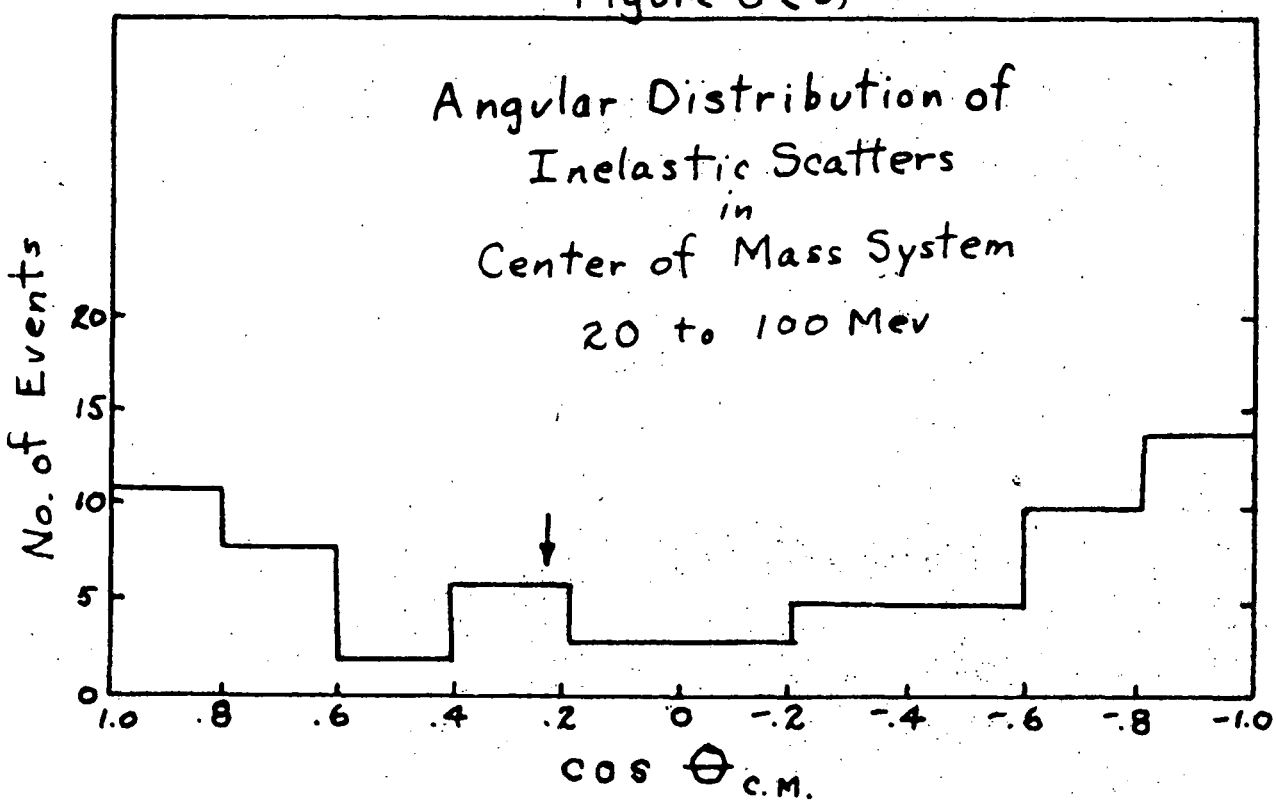

In each energy interval there is a definite backward peaking, especially pronounced for the high energy region. The arrows in Figures 7 and 8 indicate the effective average cut-off angle defined by the cross section reduction due to the Pauli exclusion principle.[37] The presence of an appreciable number of scatters at small angles in spite of the expected reduction due to the Pauli exclusion principle leads one to suspect either that the angular distribution is also peaked forward or that the Fermi motion is more important for these scatters and cannot be neglected in the conversion to the center of mass.

VI. DIFFERENTIAL ELASTIC CROSS SECTIONS

Part of the general program in investigating K meson interactions involves a study of the small angle scattering spectrum. As was indicated by the early results of Phase I of this experiment[15,16] there seemed to be more elastically scattered K mesons in the region 20° to 40° than were predicted by pure Coulomb scattering for emulsion nuclei. It was felt that additional data at smaller angles and further calculations assuming nuclear potentials were necessary for definite conclusions. In the meantime, using this information, Osborne[39] attempted to interpret the data using the Born approximation and evaluating scattering amplitudes by comparing with the inelastic data at large angles. The sign of the interference term between nuclear and Coulomb forces was found to be negative for best fit, i.e., an attractive potential. Later work using the same type of analysis indicates a repulsive potential.[40]

For Phase II of this experiment, this problem was given special attention. As mentioned in the scanning procedure, while following K meson tracks space angles were measured for all scatters with a projected angle (in the plane of the emulsion) of 2° or greater. The energy of the scatter, if elastic, was determined from the residual range after the scatter. This data was considered in the two energy intervals 40 to 100 Mev and 100 to 220 Mev. Scatters in the energy region less than 40 Mev were neglected for two reasons. Since most of the scatters are pure Coulomb and there are many of them, there is a tendency to dilute the effect of any interference which would be obvious at larger energies in the same compilation. Further, it was found that the efficiency for observing small angle scatters decreases with energy.

The rigorous cut-off at 2° was necessary since smaller angles are generally not efficiently observed. This made necessary a geometric efficiency correction. This correction was made by weighting the number of scatters at each angle by the efficiency for observing a scatter at that angle. The success of these corrections was checked by noting that the experimentally observed cross sections for angles less than 5° agreed with the cross sections predicted for point charge emulsion nuclei.

A. Elastic Scattering, 40 to 100 Mev.

Figure 9 gives the experimentally determined differential cross section for elastic scatters for the energy interval 40 to 100 Mev in the angular interval 2° to 60°. This data is based on 18.1 meters of K track. Since the path length per energy interval decreased with energy in this interval the data was separated into six 10 Mev intervals. It was combined in such a way that a scatter in a low path length region was weighted more heavily as follows:

$$\left(\frac{d\sigma}{d\Omega}\right)_{Ave} = \frac{\frac{1}{6}\sum_{j=1}^{6} \frac{1}{L_j}\left(\frac{\Delta N}{\Delta\Omega}\right)_j}{\sum_i N_i}$$

This is an average of the six values of $\frac{d\sigma}{d\Omega}$ for each 10 Mev interval.

The dashed curve represents Rutherford scattering from point charge emulsion nuclei.

Costa and Patergnani[41] have published calculations of K meson scattering at energies from 40 to 100 Mev using the optical model. In this model the nucleus is described by means of a complex potential $V_n + iV_i$, so that the nuclear interaction of a particle is reduced to a two body problem. The real part of the potential directly determines the elastic coherent scattering. The imaginary part causes an attenuation of the intensity of the incoming particle wave. The imaginary part also contributes to the elastic scattering through shadow scattering.

The imaginary potential can be estimated by using the cross section per nucleon given earlier as 6.6 mb, uncorrected for Pauli

Figure 9

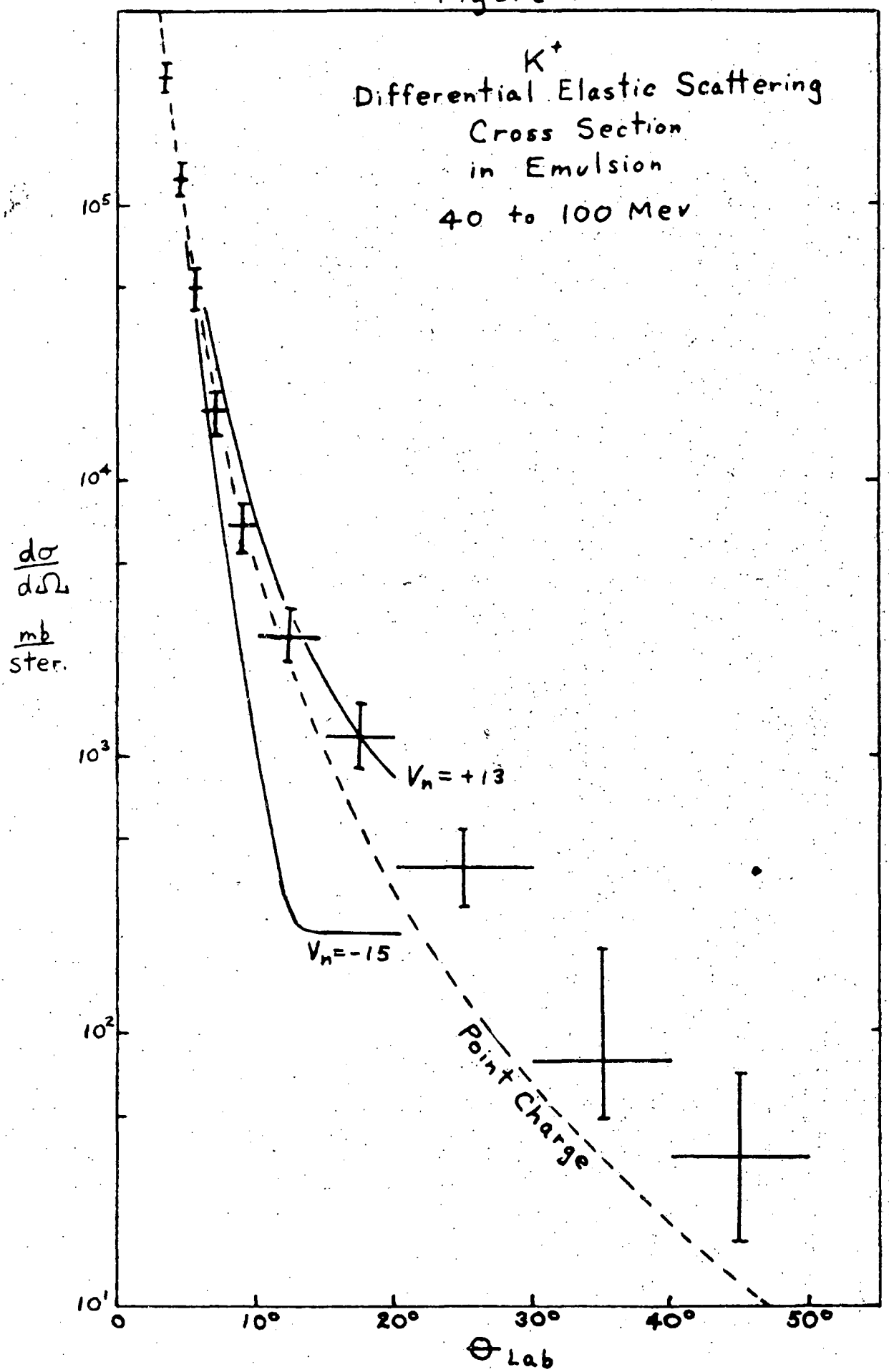
K^+
Differential Elastic Scattering
Cross Section
in Emulsion
40 to 100 Mev
$\frac{d\sigma}{d\Omega}$
$\frac{mb}{ster.}$
10^5
10^4
10^3
10^2
10^1
$V_n = +13$
$V_n = -15$
Point Charge
0
10°
20°
30°
40°
50°
θ_{Lab}

exclusion effects. The relation between the parameters is[42]

$$V_i = -\frac{\hbar v}{2 l_c} = -\frac{\hbar v \bar{\sigma}}{8/3 \pi r_0^3} = -4.7 \text{ Mev} \qquad (A-2)$$

where l_c is the mean free path in nuclear matter and r_0 = 1.2 Fermis.

Costa and Patergnani neglected the imaginary potential with the argument that its contribution to the elastic scattering would be small.

It is assumed that the potential for the inner region of the nucleus is:

$$V_r' = \frac{Ze^2}{R}\left[3/2 - 1/2\left(\frac{r}{R}\right)^2\right] + V_n \qquad (A-3)$$

that is, the potential due to a uniform distribution of electric charge plus a constant real nuclear potential V_n; in the external region

$$V_r'' = \frac{Ze^2}{r} \qquad (A-4)$$

They used the expression given by Schiff[43] for the differential cross section for the scattering of a particle by a modified coulombian field. The phase shifts, representing the deviation from the coulomb functions of the wave functions of the particle scattered by the field due to the nuclear potential, were calculated by means of the W.K.B.J. approximation method. With these phase shifts they calculated the differential cross sections in emulsion for four values of the kinetic energy of the K meson (T = 40, 60, 80, and 100 Mev) for various values of V_n.

Their results have been combined appropriately for this data and plotted as the two solid curves in figure 9. The curves for $V_n = +13$ and $V_n = -15$ Mev are given for comparison.

Clearly the curve for a repulsive potential at 13 Mev is a good fit. This is strong evidence for the presence of a nuclear potential which acts in a repulsive way on K mesons.

B. Elastic Scattering, 100 to 220 Mev.

Figure 10 gives the experimentally determined differential cross section for elastic scatters for the energy interval 100 to 220 Mev in the angular interval 2° to 50°. This data is based on 75.8 meters of K meson track. In this data the path length per 10 Mev interval fell gradually to zero at high energies so the weighting by path length was not used. The data was divided into three intervals and calculations made at three energies and each cross section weighted by the path length studied at that energy as follows:

$$\left(\frac{d\sigma}{d\Omega}\right)_{Ave.} = \sum_{j=1}^{3} f_j \left(\frac{d\sigma}{d\Omega}\right)_j$$

where $f_j = L_j / \sum L_j$ and the three values of f_j and energy intervals are given on the graph.

The dashed curve represents Rutherford scattering from point charge emulsion nuclei.

The nuclear potential necessary to explain this data has not yet been determined. However, an extensive series of calculations are presently being made by G. Igo, G. Ravenhall, and J. Teiman of Stanford University in conjunction with this group to explain both the high and low energy data. The Stanford group has made some preliminary calculations using the Born approximation and assuming that the imaginary potential could be neglected. The results of this work, obtained quite independently, showed that the low energy differential cross section agreed very well with the data if a real potential of +12 Mev was assumed. The calculation in progress now is an exact phase shift analysis using both real and

Figure 10

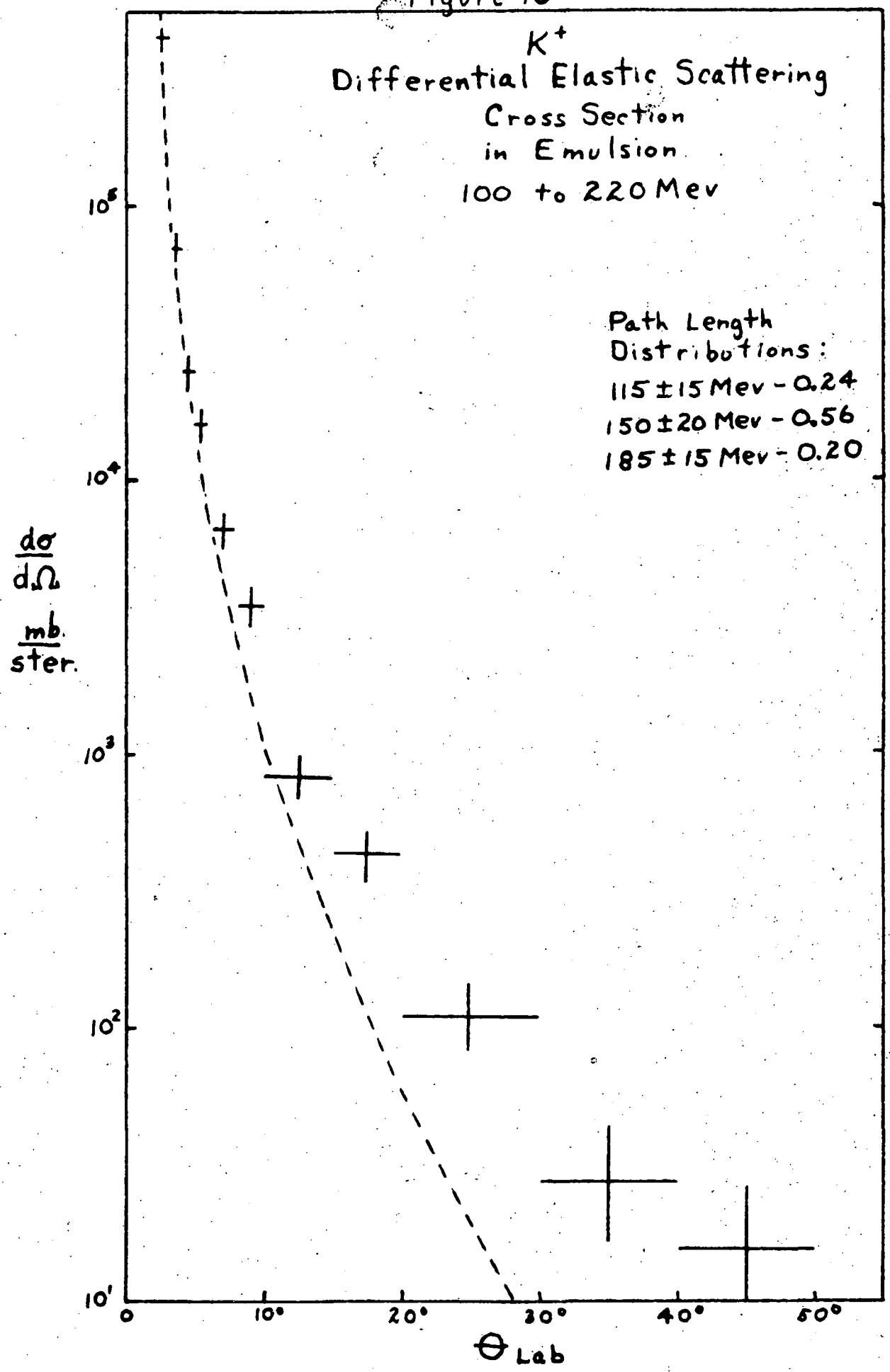
K^+
Differential Elastic Scattering
Cross Section
in Emulsion
100 to 220 Mev
Path Length
Distributions:
115 ± 15 Mev - 0.24
150 ± 20 Mev - 0.56
185 ± 15 Mev - 0.20
$\frac{d\sigma}{d\Omega}$
$\frac{mb.}{ster.}$
10^5
10^4
10^3
10^2
10^1
0
10°
20°
30°
40°
50°
θ_{Lab}

imaginary potentials and employing the computer facilities of the Los Alamos Scientific Laboratory. Both methods use the optical model discussed previously but the potentials are shaped to correspond to the charge distributions found by electron scattering[44], i.e.,

$$V(r) = V_c(r) + \frac{V_n + iV_i}{\left[1 + \exp\left(r - R/D\right)\right]}$$

where $R = 1.07 \times 10^{-13} A^{1/3}$ cm. and $D = 0.55 \times 10^{-13}$ cm. The final results of this work are not available, but several interesting features are already indicated. The introduction of the imaginary potential seems to make the difference between the predictions based on repulsive and attractive real potentials less striking. In addition, the presence of a real potential has an appreciable effect on the effective beam intensity of K mesons passing through the nucleus. This consideration could alter the cross section per nucleon derived earlier by as much as ten to twenty percent depending on the magnitude of the potential necessary.

It is also clear that the imaginary potential is no longer negligible unless the real potential has increased. An estimate based on the relation given on page 50 gives $V_i = -8$ Mev.

Another important effect which has not been thoroughly investigated yet is the possible excitation of low-lying nuclear levels. Strauch and Titus[45] have shown that this process arises in the scattering of 90 Mev protons with a frequency corresponding to about 5% of the elastic cross section. The techniques of this experiment would detect most of the nuclear excitations of the light elements in emulsion, but

most of the interactions take place with the heavy elements whose nuclear energy levels are known to be more low-lying and closer spaced than those of the light elements. These inelastic processes would have been classified as elastic in this experiment and could result in an over-estimation of the elastic differential cross section. However, preliminary estimates of the effect indicate that the proportion of such interactions is small and well within the statistical errors of the data.

VII. TOTAL CROSS SECTIONS

Using the results of the previous section it is possible to calculate the total cross section for scattering in emulsion. The total cross section is given by

$$\sigma_t = \sigma_d + \sigma_r$$

where σ_d is the elastic scattering cross section and σ_r is the combined cross section for inelastic scattering and charge exchange scattering. σ_r is called the reaction cross section .

Fernbach, Serber, and Taylor [46], in presenting their treatment of the optical model, have derived the total elastic scattering cross section. They give

$$\frac{\sigma_d}{\pi R^2} = 1 + \frac{1}{2K^2R^2}\left[1 - (1+2KR)e^{-2KR}\right] - \frac{1}{\left(\frac{K^2}{4}+k_1^2\right)^2 R^2} \times \left\{ \left(\frac{K^2}{4} - k_1^2\right) + e^{-KR}\sin 2k_1R\left[2k_1R\left(\frac{K^2}{4}+k_1^2\right) + k_1K\right] - e^{-KR}\cos 2k_1R\left[\left(\frac{K^2}{4}-k_1^2\right) + KR\left(\frac{K^2}{4}+k_1^2\right)\right]\right\}$$

where $K = 1/\ell_0$, ℓ_0 = collision mean free path in nuclear matter, R is the nuclear radius $r_0A^{1/3}$, r_0 = 1.2 Fermis, $k = p/\hbar$ is the propagation vector of the wave outside, $k + k_1$ is the propagation vector inside, $k_1 = k\left[(1 - V/T)^{\frac{1}{2}} - 1\right]$, V is the mean potential energy of the projectile inside the nucleus, and T is the kinetic energy.

The data has been divided into the two energy intervals 20 to 100 Mev and 100 to 220 Mev with mean energies of 70 Mev and 150 Mev, respectively. Since the magnitude of the repulsive potential has not as

yet been definitely established, the diffraction cross section has been calculated assuming values of 10, 20, and 30 Mev. The appropriate cross section per nucleon and reaction cross section for each interval was held constant. This is not rigorously correct for the cross section per nucleon but is sufficient for a first approximation.

The results are given in the following table:

Mean Incident Energy	Reaction Cross Section	Cross Section Per Nucleon	Total Cross Section		
			V = 10 Mev	V = 20 Mev	V = 30 Mev
70 Mev	205 mb	6.6 mb	430 mb	840 mb	1360 mb
150 Mev	284 mb	9.6 mb	430 mb	670 mb	920 mb

For comparison, the geometric cross section for emulsion has been calculated using $r_o = 1.2$ Fermis and the result is 555 mb.

VIII. ENERGY LOSS BEHAVIOUR

The first suspicion that the nuclear potential was repulsive came from observation of the fact that the K^+ meson always came out of a nuclear interaction with an appreciable energy, that is, more than the Coulomb barrier energy of 10 Mev. Of the 232 non-charge exchange inelastic events observed here, except for two cases (at 15 Mev and 23 Mev), all had final energies above 25 Mev. In addition, the energy losses were generally low, in contrast to positive π mesons where the contrary is true. In this section several observations are made of the behaviour of the fractional energy losses of K mesons which scattered inelastically.

Figure 11 shows the distribution of the fractional energy losses as a function of the laboratory angle of the scattered K. This plot includes only the data in the energy interval 100 to 220 Mev. Events below the 10% cut-off were classified as elastic unless there were prongs. Curve A represents the energy loss versus laboratory angle for K mesons on free protons. The curve is for K's of 150 Mev but is essentially the same for those from 100 to 220 Mev. There is a rather striking rise of the data points with increasing angle that roughly follows the free proton curve. Curve D for scattering from free alphas is also shown. If one assumes, as is indicated, that the K interaction is with a single nucleon in the nucleus the spread could be due to the Fermi motion of the nucleons. Assuming a maximum Fermi momentum of 218 Mev/c, curves B and C were calculated for the two cases when the K and nucleon are opposing (B) and when they are in the same direction (C). This envelope of curves B and C seems to enclose a major portion of the points. This angle-energy loss correlation is further indication that

Figure 11

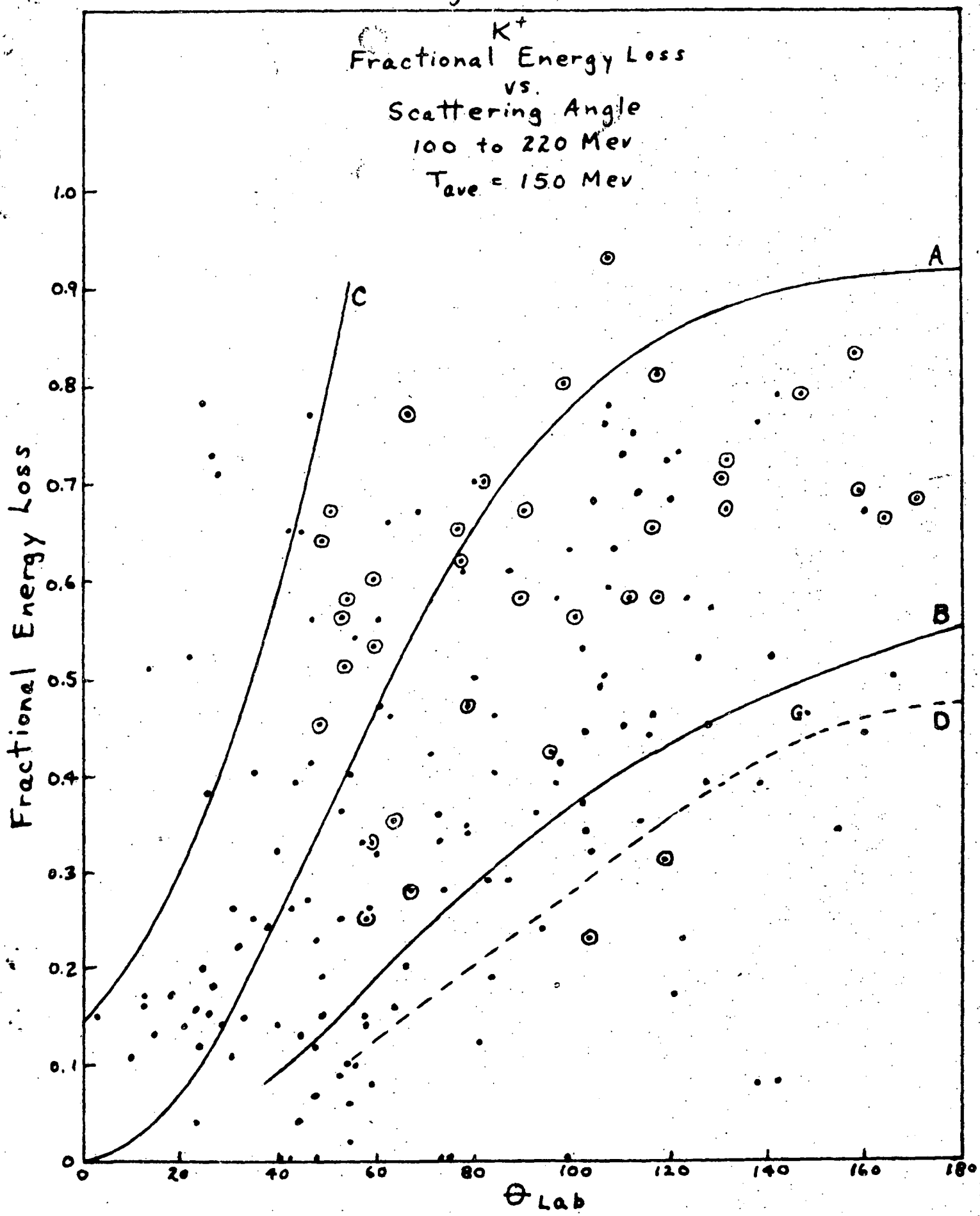
K^+
Fractional Energy Loss
vs.
Scattering Angle
100 to 220 Mev
T_{ave} = 150 Mev
Fractional Energy Loss
θ_{Lab}
A
B
C
D
0
0.1
0.2
0.3
0.4
0.5
0.6
0.7
0.8
0.9
1.0
0
20
40
60
80
100
120
140
160
180

the K interaction is with a single nucleon in the nucleus. In this connection, those cases when a high energy (knock-on or cascade) proton came out of the interaction are circled. In most of these events the proton had almost all the energy lost by the K meson so that the scatters could be classified as quasi-elastic. The fact that the points representing this type of event are uniformly interspersed among the rest leads one to believe that in the other cases the same could be true but the proton interacted again before leaving the nucleus or the original interaction was with a neutron.

Figure 12 was made by plotting the mean of the fractional energy losses in 20° intervals. Events below 40° are not included because the data is strongly influenced by the Pauli exclusion principle and the 10% energy resolution. It is possible to see that the data is consistent with a repulsive potential by using a simple model. It is assumed that the K meson experiences a potential V on entering the nucleus, so the kinetic energy before scattering is $T_i - V$. The K scatters from a nucleon at rest at an angle equal to the angle observed outside the nucleus. The outgoing K then leaves the nucleus with an energy of $T_f + V$. With this model, fractional energy losses versus angle were calculated and plotted for V =+30 and+60 Mev. The effect is clear. A repulsive potential gives the suppression desired to agree with the data. The magnitude of V for best fit is not significant since the motion of the nucleons has been neglected.

In Figure 13 the mean fractional K meson energy loss is plotted in 20 Mev incident energy intervals. In order to make an estimate

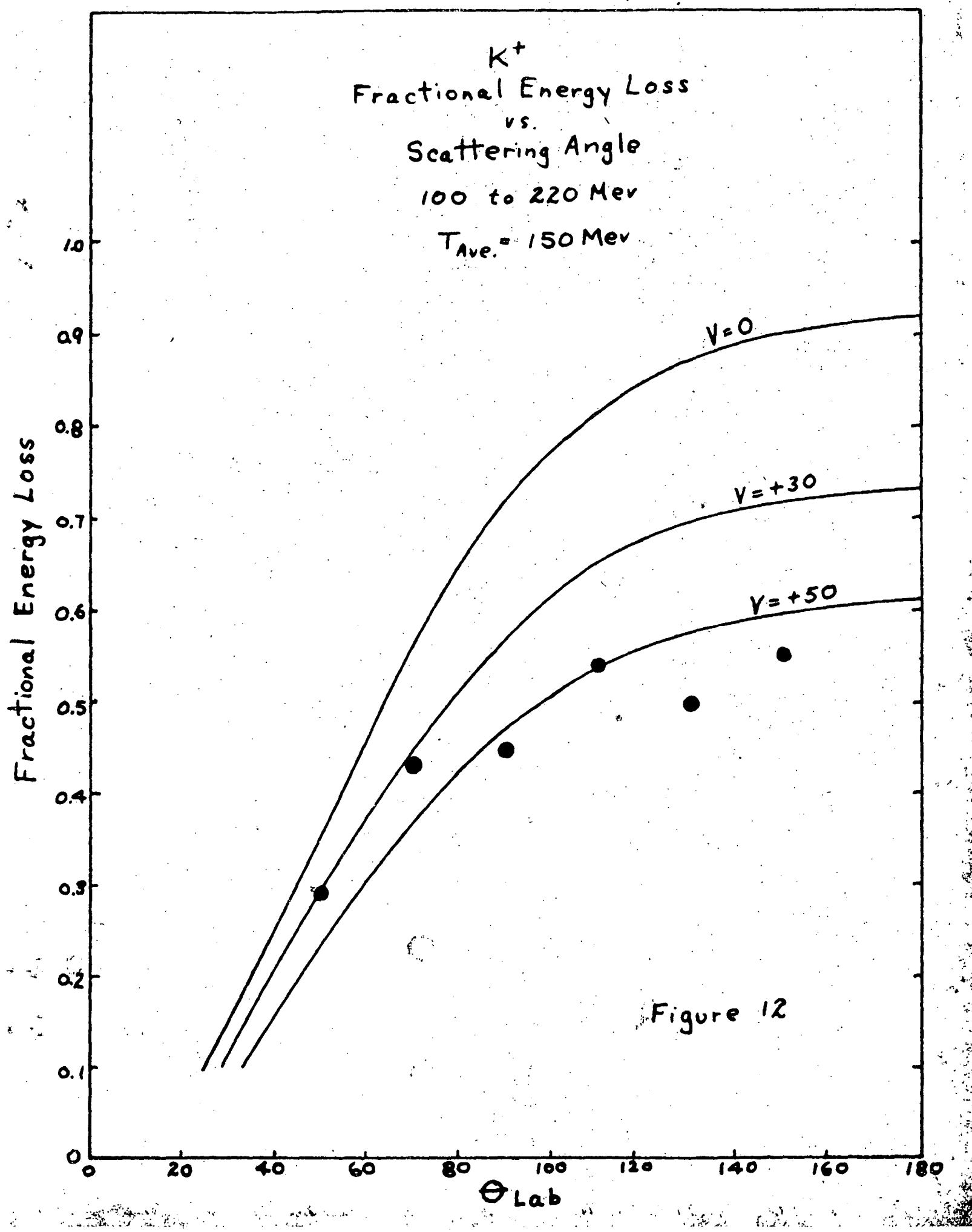
K+
Fractional Energy Loss
vs.
Scattering Angle
100 to 220 Mev
T Ave. = 150 Mev
V=0
V=+30
V=+50
Fractional Energy Loss
1.0
0.9
0.8
0.7
0.6
0.5
0.4
0.3
0.2
0.1
0
0
20
40
60
80
100
120
140
160
180
θ Lab

Figure 12

of the expected energy losses with various nuclear potentials the following model was used. On entering the nucleus the K meson experiences a potential V which is the sum of the nuclear and coulomb potentials. At this reduced energy it interacts with a single nucleon. Assuming that the angular distribution of the K-nucleon scatters is isotropic in the center of mass system, the most probably angle of scatter is that at 90° in the center of mass due to solid angle considerations. However, the Pauli exclusion principle prevents a fraction of the scatters at small angles so that the mean angle of scatter is really greater than 90° and varies with incident energy. Assuming that the nucleon must be given a momentum greater than 200 Mev/c, these mean angles were estimated. Then each mean angle of scatter gave a certain mean energy loss. The final kinetic energy was then increased by the amount V to correspond to the energy observed outside the nucleus and then the observed fractional energy loss predicted. The predictions as a function of incident energy are shown as solid curves on Figure 13 for several values of V. The best fit is for V =+30 Mev. The feature of most significance is that the data indicates a repulsive potential above that of Coulomb repulsion.

Figure 13

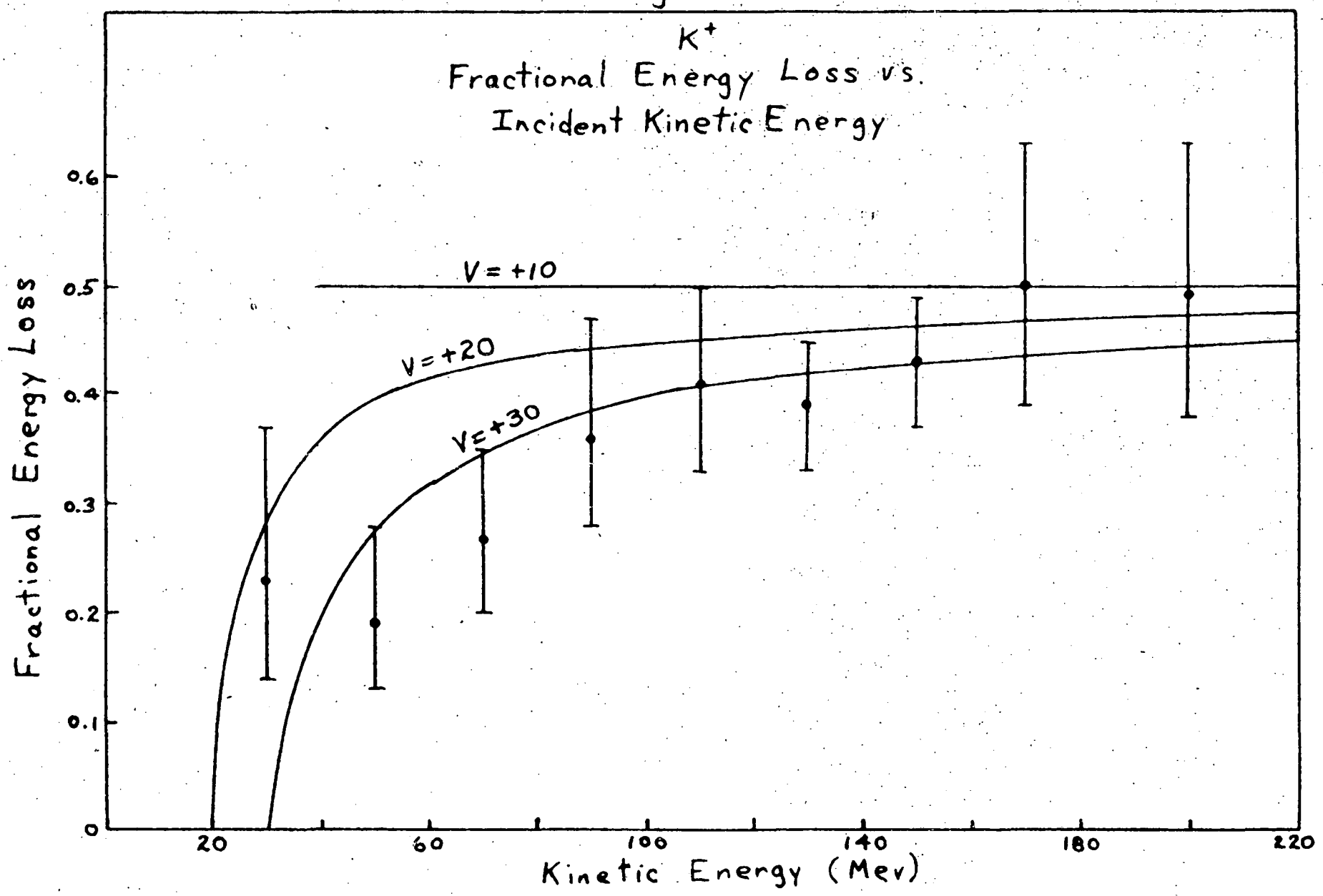
K^+
Fractional Energy Loss vs.
Incident Kinetic Energy
V = +10
V = +20
V = +30
Fractional Energy Loss
0
0.1
0.2
0.3
0.4
0.5
0.6
20
60
100
140
180
220
Kinetic Energy (Mev)

IX. NUCLEAR EXCITATION

Systematic studies of the number, type, and energy and angular distribution of star prongs resulting from the collisions in flight of various particles with emulsion nuclei have been made in a number of experiments.[47] In general, the indications are that star formation proceeds in two steps: (1) the "fast" ($\sim 10^{-22}$ sec) initial catastrophic process which includes nucleon scattering in the nucleus (usually called the cascade or knock-on process), pickup, stripping, charge exchange, and meson production, and (2) then the "slow" ($\sim 10^{-20}$ sec) de-excitation of the resulting nucleus usually termed the evaporation process.

An analysis in these terms is made for this data in order to understand better the initial K-nucleon collision process and the distribution of the energy lost by the K meson.

For this type of analysis, K^+mesons have several desirable properties: the conservation of strangeness in strong interactions, the lack of any other strange particle channel, and (except for charge exchange collisions) the absolute identification of the K meson among the star prongs by virtue of its different mass and its decay process.

The prongs of K meson stars (i.e., prongs other than the K meson coming in and going out) can be put into one of three length classes: (a) $R < 10\mu$, (b) $10\mu \leq R \leq 1.2$ mm. and (c) $R > 1.2$ mm. Class (a) includes recoils, delta rays, and low energy alphas or protons which leaked through the Coulomb barrier. Class (b) primarily includes protons and has been examined in terms of an evaporation spectrum. In two stars, a prong appeared straighter, was thicker, and showed a few delta rays.

These were assumed to be alphas and the stars were excluded from the evaporation analysis. Class (c) includes primarily high energy protons.

Stars formed by K mesons having energies between 100 to 220 Mev were analyzed and Figure 14 shows a histogram of the energy distribution of all protons with ranges greater than 10μ and having energies less than 50 Mev.[48] (This data includes only that obtained in scanning at Berkeley.) Clearly it indicates the familiar Maxwellian distribution of proton energies characteristic of evaporation processes, plus the long tail of knock-on or cascade protons.

It has been shown[49,50] that such evaporation spectra can be represented by the relation

$$N(T)\,dT = N_0 \frac{T-V}{\tau^2} e^{-\frac{T-V}{\tau}} dT$$

where T is the kinetic energy of the prong, τ is the nuclear temperature, V is the effective Coulomb barrier height, N_0 is the total number of evaporation prongs in the spectrum, and $N(T)dT$ is the number of prongs lying in the interval dT about T. This simplified version of the evaporation relations is strictly applicable only to the heavy elements at excitation energies large compared with the binding energy per nucleon.

The first consideration is to make a choice of an effective Coulomb barrier. Recently, Bailey[51] has experimentally studied the evaporation spectra of a number of elements and obtains an effective Coulomb barrier necessary for a best fit in each case. Plotting his potentials and extrapolating to obtain values for the average heavy element and the average light element one obtains values of about 4 Mev

Figure 14

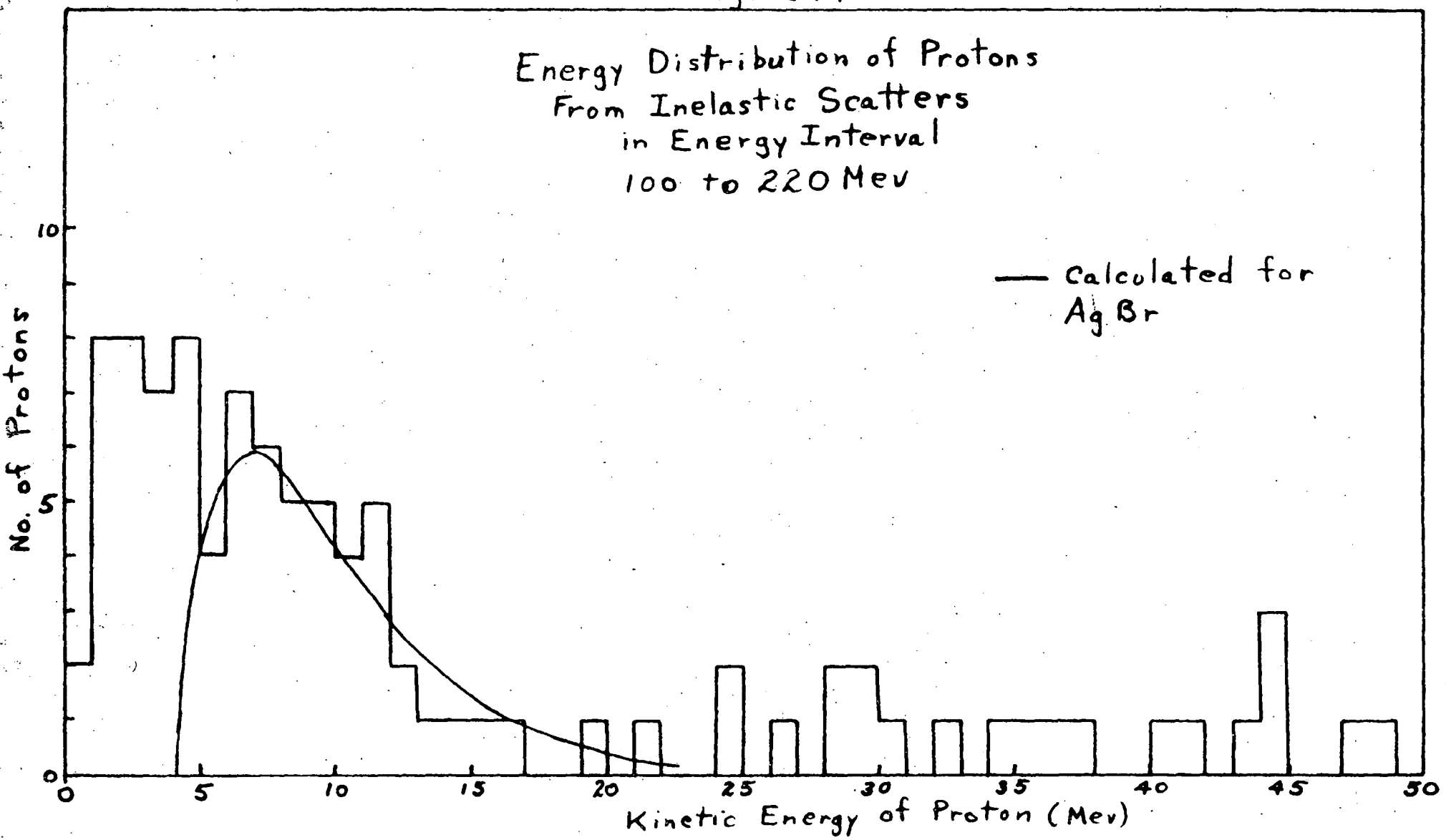
Energy Distribution of Protons
From Inelastic Scatters
in Energy Interval
100 to 220 Mev
Calculated for
Ag Br
No. of Protons
0
5
10
0
5
10
15
20
25
30
35
40
45
50
Kinetic Energy of Proton (Mev)

and zero Mev, respectively.

Therefore the histogram in Figure 14 is a composite of prongs from light elements and heavy elements with the light elements contributing predominantly to prongs having energies less than 4 Mev. Since evaporation theory cannot be applied to the light elements, only the prongs having energies greater than 4 Mev are used and it is assumed that they come mostly from the heavy elements.

The parameter τ, the nuclear temperature, was evaluated by plotting $\ln [N(T)dT/(T - V)]$ vs. T on semi-log paper using V = 4 Mev. The slope of the best fit straight line through the points between 4 to 20 Mev gave a τ of 2.9 Mev. The predicted distribution using this temperature is also given in Figure 14.

From evaporation theory, it is shown[50,52] that the excitation energy of a nucleus can be represented approximately by $W = A\tau^2/10$. Hence the excitation energy is 79 Mev.

The mean energy loss for K mesons in the energy interval 100 to 220 Mev has been found to be 67 Mev. The correspondence is good. The smaller value for the mean energy loss could be due to the inclusion in that determination of events with small energy losses when the evaporation of one or two neutrons was the most likely manner of cooling.

From these observations, it can be concluded that the star energies can be satisfactorily accounted for by the kinetic energy losses of the K mesons.

X. SCATTERING AMPLITUDE ANALYSIS

From the available data on complex nuclei one can obtain some information on the elementary K-nucleon cross sections in terms of the scattering amplitudes.

It is assumed that in the range of energies investigated the S and P states are primarily responsible for the scattering and that states of higher momentum do not play a significant role. This is reasonable since the impact parameter, ka (where $k = 1/\lambda\!\!\!^{-}$ is the wave number and a is the radius of a nucleon), varies roughly from one to two for K's at these energies.[53]

The differential cross section for the scattering of a spin-zero particle by a spin-$\frac{1}{2}$ particle is [54,55]

$$\frac{d\sigma}{d\Omega} = \lambda\!\!\!^{-2}\left(A + B\cos\theta + C\cos^2\theta\right) \qquad (X-1)$$

and the total cross section is

$$\sigma = 4\pi\lambda\!\!\!^{-2}\left(A + \tfrac{1}{3}C\right) \qquad (X-2)$$

where

$$\begin{aligned} A &= |a_s|^2 + |a_{p1} - a_{p3}|^2 \\ B &= 2\,\mathrm{Re}\, a_s^*(2a_{p3} + a_{p1}) \\ C &= |2a_{p3} + a_{p1}|^2 - |a_{p3} - a_{p1}|^2 \end{aligned} \qquad (X-3)$$

a_S is the S wave scattering amplitude, a_{P3} and a_{P1} are the amplitudes of the scattered $P_{3/2}$ and $P_{1/2}$ waves. Also $a = \sin\delta e^{i\delta}$, where δ is the phase shift. However, these relations apply directly only to

processes that proceed through a single isotopic spin state. Using the isotopic spin assignment of $T = \frac{1}{2}$ proposed for the K meson[13], scattering can occur off a proton in the $T = 1$ state and off a neutron in both the $T = 0$ and $T = 1$ states. Assuming the validity of charge independence, the possible reactions and the isotopic spin amplitude combinations which replace the amplitudes in equation X-3 are

Reaction	Amplitude	Reaction Reference Symbol
$K^+ + P \rightarrow K^+ + P$	a_1	P+
$K^+ + N \rightarrow K^+ + N$	$\frac{1}{2}(a_1 + a_o)$	N+
$K^+ + N \rightarrow K^o + P$	$\frac{1}{2}(a_1 - a_o)$	No

where a_1 and a_o represent the $T = 1$ and $T = 0$ scattering amplitudes, respectively.

It is convenient at this point to adopt the following notation similar to that common in π meson physics: The S wave scattering amplitudes of $T = 0$ and $T = 1$ will be indicated by a_0 and a_1. The P wave scattering amplitudes will be indicated by a_{01}, a_{11}, a_{03}, a_{13}, where the first index is the isotopic spin of the state in question and the second index is twice the angular momentum. The angular distribution coefficients for the three possible reactions become

$$A_{P+} = |a_1|^2 + |a_{11} - a_{13}|^2$$
$$B_{P+} = 2\mathrm{Re}\, a_1^*(2a_{13} + a_{11})$$
$$C_{P+} = |2a_{13} + a_{11}|^2 - |a_{13} - a_{11}|^2$$

$$A_{N+} = \tfrac{1}{2}|a_1 + a_0|^2 + \tfrac{1}{4}|a_{11} + a_{01} - a_{13} - a_{03}|^2$$

$$B_{N+} = \tfrac{1}{2}\mathrm{Re}\,(a_1 + a_0)^*(2a_{13} + 2a_{03} + a_{11} + a_{01})$$

$$C_{N+} = \tfrac{1}{4}|2a_{13} + 2a_{03} + a_{11} + a_{01}|^2 - \tfrac{1}{4}|a_{13} + a_{03} - a_{11} - a_{01}|^2$$

$$A_{No} = \tfrac{1}{2}|a_1 - a_0|^2 + \tfrac{1}{4}|a_{11} - a_{01} - a_{13} + a_{03}|^2$$

$$B_{No} = \tfrac{1}{2}\mathrm{Re}\,(a_1 - a_0)^*(2a_{13} - 2a_{03} + a_{11} - a_{01})$$

$$C_{No} = \tfrac{1}{4}|2a_{13} - 2a_{03} + a_{11} - a_{01}|^2 - \tfrac{1}{4}|a_{13} - a_{03} - a_{11} + a_{01}|^2$$

Direct evidence for the reaction $K^+ + P \rightarrow K^+ + P$ is provided by the K-P interactions discussed in Section IV. It is seen that the total cross section is rather constant from 20 to 200 Mev. The angular distribution appears to be isotropic in the center of mass. This behaviour is characteristic of pure S wave scattering and is a strong indication that the P wave scattering in the T = 1 state is zero or small at these energies (below 200 Mev). This observation was also made by other authors[17,18,35] upon examining the earlier, more limited, results on the K-P angular distribution and energy dependence below 140 Mev. This work extends the data to 200 Mev and gives the angular distribution with better statistics. Using this information we make the assumption that there are no P wave contributions to the $K^+ + P$ scattering. Thus we can set a_{13} and a_{11} equal to zero.

Since the available experimental data is not sufficient to distinguish the two P wave scattering states ($P_{3/2}$ and $P_{1/2}$), several simplifying assumptions are made regarding the relative magnitude of the

two amplitudes a_{01} and a_{03}.

Case I: $a_{01} = a_{03}$

This assumption is equivalent to the statement that there is no spin-orbit coupling and hence no "spin flip".

Case II: $a_{01} = -\frac{1}{2} a_{03}$

This assumption is based on the cut-off theory of Chew and is suggested by Stapp in UCRL-3535.[66] It is an approximation which applies when the phase shifts are small.

Setting the T = 1 state P wave amplitudes equal to zero and applying Case I, the angular distribution coefficients become

$$A_{P+} = |a_1|^2$$

$$B_{P+} = 0$$

$$C_{P+} = 0$$

$$A_{N+} = \tfrac{1}{4}|a_1 + a_0|^2$$

$$B_{N+} = (3/2)\ \mathrm{Re}\ (a_1 + a_0)^* a_{03}$$

$$C_{N+} = (9/4)\ |a_{03}|^2$$

$$A_{No} = \tfrac{1}{4}|a_1 - a_0|^2$$

$$B_{No} = -(3/2)\ \mathrm{Re}\ (a_1 - a_0)^* a_{03}$$

$$C_{No} = (9/4)\ |a_{03}|^2$$

Similarly for Case II the angular distribution coefficients become

$$A_{P+} = |a_1|^2$$

$$B_{P+} = 0$$

$$C_{P+} = 0$$

$$A_{N+} = \tfrac{1}{4}|a_1 + a_0|^2 + (9/16)|a_{03}|^2$$

$$B_{N+} = (3/4)\ \mathrm{Re}\ (a_1 + a_0)^* a_{03}$$

$$C_{N+} = 0$$

$$A_{No} = \tfrac{1}{4}|a_1 - a_0|^2 + (9/16)|a_{03}|^2$$

$$B_{No} = -(3/4)\ \mathrm{Re}\ (a_1 - a_0)^* a_{03}$$

$$C_{No} = 0$$

In comparing these results with the experimental data several interesting implications arise.

The above relations predict that the differential cross section for K-neutron scattering peaks forward or backward as soon as the P wave scattering becomes appreciable. As shown in Figure 8 the experimental angular distribution of the inelastic scatters from complex nuclei when transformed to the center of mass system peaks backward. Since the angular distribution of the K-P scatters from free protons appears to be isotropic, this backward peaking must be due to the neutrons. Further, since the K's are visible after the scatter the backward peak must be due to the direct scattering reaction on neutrons. This agrees

with both of the above cases if the real part of the product $(a_1 + a_0)^* a_{03}$ is negative.

Since the calculations of the K-neutron direct scattering and charge exchange cross sections assumed an isotropic distribution in the center of mass in order to correct for the exclusion principle, it is clear that these estimates should be altered. This is especially true in the high energy interval where P wave scattering is important. The alteration would make estimations of both cross sections larger. The observation in Section V-B that the average K-nucleon cross section was roughly constant up to 200 Mev was evidently only apparent. The P wave increase at small angles must have been reduced by the Pauli exclusion effect.

The ratio of the charge exchange cross sections to the non-charge exchange cross sections in the two cases become

Case I:

$$\frac{\sigma_{No}}{\sigma_{P+} + \sigma_{N+}} = \frac{\frac{1}{4}|a_1 - a_0|^2 + (3/4)|a_{03}|^2}{|a_1|^2 + \frac{1}{4}|a_1 + a_0|^2 + (3/4)|a_{03}|^2}$$

Case II:

$$\frac{\sigma_{No}}{\sigma_{P+} + \sigma_{N+}} = \frac{\frac{1}{4}|a_1 - a_0|^2 + (9/16)|a_{03}|^2}{|a_1|^2 + \frac{1}{4}|a_1 + a_0|^2 + (9/16)|a_{03}|^2}$$

In the limiting case of pure S wave scattering at low energies the two cases are the same, i.e.,

$$\frac{\sigma_{No}}{\sigma_{P+} + \sigma_{N+}} \rightarrow \frac{\frac{1}{4}|a_1 - a_0|^2}{|a_1|^2 + \frac{1}{4}|a_1 + a_0|^2}$$

the coefficient of the cos θ term of the charge exchange angular distribution must be positive. This requires that the charge exchange distribution peak forward.

Observation of this effect in this experiment is still under investigation. It is expected that a forward distribution of scatters would result in lower average nuclear excitation for charge exchange scatters. This does not mean necessarily that the number of prongs of these stars will be less because the existence of a proton excess in this type of event increases the probability for proton emission in the evaporation spectra. Scanning is still in progress to find charge exchange scatters and an analysis similar to that of Section IX will be made when sufficient data is available. However, preliminary estimates based on the data given in this report indicate that the nuclear excitation for charge exchange stars is about one-half that for ordinary inelastic events.

It can be concluded therefore that a forward distribution of the charge exchange scatters also agrees with the experimental data available at present.

XI. ACKNOWLEDGMENTS

I am deeply grateful to Professor Gerson Goldhaber for his encouragement, guidance, and aid throughout my graduate work. It is also a pleasure to thank Dr. Sulamith Goldhaber for her continued interest and assistance. My thanks are due to Dr. Warren Chupp, Dr. Edwin Iloff, and Mr. Francis Webb for their many contributions and helpful suggestions. I am indebted to Dr. Donald H. Stork for his guidance and assistance in designing and setting up the separated K beam. For their contributions and cooperation I would also like to thank Dr. Aihud Pevsner and Dr. David Ritson of the Massachusetts Institute of Technology and Dr. G. Puppi and Dr. G. Quareni of the University of Bologna. Thanks are due to each of the many scanners who worked so diligently in locating the K mesons and making many of the measurements.

This work was done under the auspices of the United States Atomic Energy Commission.

APPENDIX A

Composition of Emulsion:

Below are listed the emulsion ingredients as given by the manufacturer of G-5 emulsion, Ilford, Inc., August 1955. The density measurements were made at 58% relative humidity.

Element	Density (ρ)	Z	A	ρ/A	$\rho/A^{1/3}$
Ag	1.831 ± 0.030	47	107.9	0.0170	0.385
Br	1.349 ± 0.020	35	79.92	0.0169	0.314
C	0.276 ± 0.005	6	12.01	0.0230	0.121
O	0.249 ± 0.004	8	16.00	0.0156	0.099
N	0.073 ± 0.001	7	14.01	0.0052	0.033
H	0.0533 ± 0.0009	1	1.008	0.0529	0.053
I	0.012	53	126.9	0.0001	0.002
S	0.007	16	32.07	0.0002	0.002
Total	3.850 ± 0.041			0.1309	1.009

The approximation to emulsion used in most of the calculations of this work was as follows:

Element	Density (ρ)	Z	A	ρ/A	$\rho/A^{1/3}$
Ag	1.831	47	107.9	0.0170	0.385
Br	1.349	35	79.92	0.0169	0.314
C-N-O	0.598	7	13.7	0.0438	0.253
H	0.0533	1	1.008	0.0529	0.053

ρ/A is proportional to the number of atoms of each element present per cubic centimeter through the relation $N_i = (\rho_i/A_i)L$ where L is Avegadro's number. $\rho/A^{1/3}$ is proportional to the geometrical cross section presented by each element in a thickness of one centimeter through the relation

$$N_i\sigma_{oi} = (\rho_i/A_i)L\,\pi r_o^2\,A^{2/3} = (\rho_i/A_i^{1/3})L\,\pi r_o^2 .$$

APPENDIX B

Data obtained in Phase I:

Table IV gives all events found which had a scatter greater than 40° (i.e., elastic and inelastic) and those events which scattered less than 40° but were obviously inelastic (i.e., had prongs or a visible grain density change). The charge exchange events are also given. The K-hydrogen events are easily distinguished and are given separately in Section IV. This list includes the data resulting from the study of 12 meters of track at M.I.T. and 24.5 meters at U. of C., Berkeley, in the energy interval 30 to 120 Mev.

Column 1 gives the code reference for the event.

Column 2, θ gives the space angle of the scatter (i.e., the angle between the track made by the incoming K and the track made by the outgoing K). The rms error on each of these measurements is of the order of one degree. This error is primarily due to the variation in the correct shrinkage factor to be used in evaluating the dip angles. The thickness of a developed plate varies somewhat with humidity. Charge exchange events are listed in this column as C.E.

Column 3, T_i, gives the kinetic energy of the incoming K meson. Here it is evaluated by comparing with the known residual range of the K's in the same region of the plate which did not make any inelastic collision.

Column 4, T_f, gives the kinetic energy of the K meson as it leaves the interaction. It was determined by either the observed residual range (indicated by small errors) or by a grain count immediately after the scatter. In those cases marked by an asterisk, the information is not

available to us.

Column 5 gives the identity and range of star prongs other than the K meson. Identification of prongs with range less than 100μ is very difficult. They were classified as protons unless they appeared unusually heavy and straight in which case they were classified as alpha particles. Prongs less than 10μ were classed as recoils if straight and heavy.

Column 6 gives the visible energy of the interaction, other than the outgoing K meson, and is obtained from the information given in Column 5. The conversion from range to energy was made using the tables distributed by W. H. Barkas[48] for low energy particles. Binding energies of 8 Mev for protons and 4 Mev for alpha particles have been included.

Column 7 gives the classification as to whether the interaction was considered elastic or inelastic. All scatters with no prongs were classed as elastic if the grain density change across the scatter indicated that the energy loss was less than 10%. Whenever a scatter had a recoil which clearly did not conserve momentum, it was classed as inelastic. If there was any suspicion that it did conserve momentum, the momentum transfer, $2p\sin\theta/2$, was evaluated from the scattering angle and known range of the K meson. For the elements of emulsion (excluding hydrogen) this is a good first approximation of the momentum of the recoiling nucleus. With this information and the range-energy plots of Reynolds and Zucker[57] for nitrogen in nuclear emulsion, it was possible to determine whether the scatter was elastic.

PHASE I - DATA

Code	θ Degrees	T_i (Mev)	T_f (Mev)	Prongs Excl. K	Visible Energy Excl. K (Mev)	Class
M20	75	35 ± 9	*	None	0	Inelastic
S9	90	42 ± 9	18 ± 1	P-1.5 mm	26	"
S43	134	42 ± 9	19 ± 1	Electron	~ 0	"
S13	145	43 ± 1	43 ± 1	None	0	Elastic
I8	94	45 ± 6	14 ± 1	P-199μ	13.5	Inelastic
M13	C.E.	47 ± 9	-	P -500μ	17.4	"
M19	30	48 ± 8	*	P-200μ	13.5	"
M14	90	49 ± 8	21	None	0	"
I5	103	49 ± 16	20 ± 1	P-1.72 mm	27.5	"
S08	93	49 ± 16	49 ± 16	None	0	Elastic
K37M	5	58 ± 8	51 ± 8	Rec	~ 0	Inelastic
S47	60	52 ± 1	52 ± 1	None	0	Elastic
K14M	63	53 ± 1	53 ± 1	None	0	"
S49	100	57 ± 1	57 ± 1	None	0	"
S8	83	62 ± 6	62 ± 6	None	0	"
M12	100	62 ± 6	4 ± 1	None	0	Inelastic
M17	161	62 ± 6	20 ± 1	P-20μ	9.3	"
M15	177	63 ± 6	25 ± 1	P-2.3mm	3.1	"
I2	C.E.	63 ± 12	-	P-615μ P-175μ P-3.86mm	71	"
M41a	58	63 ± 1	63 ± 1	None	0	Elastic
M11	45	68 ± 6	*	None	0	Inelastic

Code	θ Degrees	T_i (Mev)	T_f (Mev)	Prongs Excl. K	Visible Energy Excl. K (Mev)	Class
X5	65	68 ± 6	68 ± 6	None	0	Elastic
SC17	32	70 ± 12	70 ± 12	None	0	"
I9	95	73 ± 4	12 ± 1	P-1.7mm	27.5	Inelastic
X8	51	74 ± 12	74 ± 12	None	0	Elastic
SC14a	84	75 ± 4	75 ± 4	None	0	"
S25	87	76 ± 6	76 ± 6	None	0	"
W21	145	78 ± 6	50	None	0	Inelastic
RC25a	27	78 ± 12	78 ± 1	Rec.	0	Inelastic
W16	132	84 ± 6	*	3P's or 3α's	*	"
I1	44	84 ± 12	69 ± 1	P-4.6u P-6.9u P-7.0u P-582u	44	"
I4	C.M.	88 ± 11	-	P-203u	13.6	"
SC 1	64	88 ± 1	88 ± 1	None	0	Elastic
X10	C.M.	93 ± 5	-	P-10mm	60	Inelastic
S5	73	93 ± 13	38 ± 1	Rec-7u P-120u	15	"
X3	54	93 ± 13	93 ± 13	None	0	Elastic
SC5	51	97 ± 10	97 ± 10	None	0	"
W22	143	110 ± 5	50 ± 1	None	0	Inelastic
I3	143	112 ± 10	33 ± 1	P-137u	12	"

APPENDIX C

Data obtained in Phase II:

Table V gives all events which had a scatter greater than 40° (i.e., elastic and inelastic) and those events which scattered less than 40° but were obviously inelastic (i.e., had prongs or a visible grain density change). The charge exchange events are also included. The K-hydrogen events are given separately in Section IV. This list includes data obtained in scanning 110.6 meters of track at Berkeley from 20 Mev to 220 Mev.

Columns 1 and 2 are the event code and space angle, respectively.

Column 3 again gives the kinetic energy of the incoming K meson, however, here it is evaluated by a good grain count of the incoming track. When several determinations were available, e.g., an early grain count or a multiple scattering measurement, the weighted mean was used.

Column 4, T_f, the final kinetic energy is the same as discussed for Phase I data.

Column 5, ΔT, is the energy lost by the K meson at the scatter as determined by $(T_i - T_f)$ of columns 3 and 4.

Column 6, $\Delta T/T_i$, is the fractional energy loss.

Column 7 is the same as Column 5 of Phase I data and gives the identity and range of star prongs other than the K.

Column 8 gives the total visible energy, excluding K meson, including the binding energy of all prongs given in Column 7.

Column 9 gives the decay mode of the K meson. K_L includes the $K_{\pi 2}$, $K_{\mu 2}$ and K_{e3} decay modes. The $K_{\mu 3}$, τ, and τ' modes are indicated as such.

PHASE II - DATA

Code	θ Deg	T_i (Mev)	T_f (Mev)	ΔT	ΔT/T	Prongs Excl. K	Visible Energy Excl. K (Mev)	Decay Mode
F004	4	28 ±3	25 ±1	3 ±3	.11 ±.09	None	0	K_L
F084	75	29 ±3	23 ±1	6 ±3	.21 ±.07	None	0	K_L
F163	49	31 ±1	31 ±1	0 ±2	0 ±.08	Rec-2u	3	τ
6023	132	35 ±1	35 ±1	0 ±2	0 ±.08	Rec-1u	0	K_L
F032	46	36 ±1	36 ±1	0 ±2	0 ±.08	None	0	K_L
F096	132	44 ±5	36 ±1	8 ±6	.18 ±.08	None	0	K_L
W024	87	45 ±6	37 ±1	8 ±6	.18 ±.07	None	0	K_L
F045	48	46 ±5	31 ±1	15 ±5	.33 ±.06	None	0	K_L
F129	49	56 ±5	56 ±5	0 ±7	0 ±.08	Rec-2u	3	K_L
1015	97	57 ±1	57 ±1	0 ±2	0 ±.08	None	0	K_L
W032	59	60 ±1	60 ±1	0 ±2	0 ±.08	None	0	K_L
F069	81	60 ±8	45 ±1	15 ±8	.25 ±.08	None	0	K_L
5011	83	64 ±6	51 ±5	13 ±8	.20 ±.07	Rec-1.8u	0	Out
1040	33	66 ±7	54 ±1	12 ±7	.18 ±.08	Rec-1.3u	0	K_L
F101	151	67 ±5	46 ±1	21 ±5	.31 ±.08	None	0	K_L
1052	78	68 ±1	68 ±1	0 ±2	0 ±.09	Rec-1.3u	0	K_L
W059	44	68 ±6	39 ±1	29 ±6	.43 ±.04	P-322u	15.4	K_L
F077	41	70 ±10	59 ±1	11±10	.16 ±.08	None	0	K_L
F067	53	70 ±10	52 ±1	18 ±10	.26 ±.08	None	0	K_L
1084	46	73 ±15	73 ±15	0 ±31	0 ±.09	None	0	K_L
1062	60	74 ±6	40 ±1	34 ±6	.46 ±.04	None	0	K_L
6042	135	75 ±6	47 ±1	28 ±6	.37 ±.05	Rec-1u	0	K_L
F003	104	75 ±7	65 ±1	10 ±7	.13 ±.08	P-17.3u P-6.9u	19.1	K_L

Code	θ Deg	T_i (Mev)	T_f (Mev)	T	T/T	Prongs Excl. K	Visible Energy Excl. K (Mev)	Decay Mode
F147	46	75 ±7	65 ±7	10 ±10	.04 ±.09	None	0	K_L
6093	33	79 ±7	42 ±1	36 ±7	.41 ±.08	P-2.8mm	34	K_L
6051	56	77 ±7	66 ±1	11 ±7	.14 ±.08	None	0	K_L
6037	109	82 ±8	46 ±1	36 ±8	.44 ±.05	None	0	K_L
6014	85	84 ±1	84 ±1	0 ±2	0 ±.09	Rec-1.3u	0	K_L
6018	1	84 ±8	57 ±1	27 ±8	.32 ±.06	None	0	K_L
F015	11	85 ±8	68 ±6	17 ±10	.20 ±.05	None	0	Out
1005	62	96 ±9	51 ±1	45 ±9	.47 ±.04	P-2 mm P-5.3u	45	τ
6092	94	96 ±9	80 ±8	16 ±13	.17 ±.08	Rec-1.4u	0	Out
F113	48	98 ±10	72 ±6	26 ±12	.27 ±.07	P-776u	20	K_L
F083	138	100 ±10	92 ±1	8 ±10	.08 ±.09	Rec-4u	8	K_L
1035	148	101 ±10	45 ±1	56 ±10	.46 ±.04	Rec-1u	0	τ
6061	126	102 ±10	60 ±1	42 ±10	.41 ±.05	Rec-2.6u	4	K_L
1038	64	102 ±15	83 ±8	19 ±17	.19 ±.07	Rec-2u	3	Out
1113	108	104 ±9	57 ±1	46 ±9	.44 ±.05	Rec-4.6u	7	K_L
1018	79	104 ±10	55 ±1	49 ±10	.47 ±.05	P-3.3mm Rec-3.9u	42	K_L
F026	94	104 ±10	79 ±1	25 ±10	.24 ±.05	Rec-0.8u	0	K_L
1164	38	104 ±10	79 ±8	25 ±13	.24 ±.07	None	0	Out
F139	40	106 ±10	72 ±1	34 ±10	.32 ±.06	None	0	K_L
6043	84	107 ±10	76 ±1	31 ±10	.29 ±.07	P-75u	11	K_L
F116	28	108 ±10	67 ±1	41 ±10	.38 ±.08	None	0	K_L
1249	73	108 ±10	72 ±1	36 ±10	.33 ±.07	P-283 u P-600u	33	K_L

Code	θ Deg	T_i (Mev)	T_f (Mev)	T	T/T	Prongs Excl. K	Visible Energy Excl. K (Mev)	Decay Mode
M002	45	109 ±10	95 ±10	14 ±14	.13 ±.08	Rec-1μ	0	K_L
7033	C.E.	109 ±10	-	-	-	Rec-3μ P-23.1mm	97	-
6028	C.E.	110 ±10	-	-	-	Rec-1μ P-475μ P-140μ	29.4	-
6011	31	110 ±10	81 ±8	29 ±13	.26 ±.07	P-207μ	13.5	Out
5195	147	110 ±10	59 ±1	51 ±10	.46 ±.05	P-3.4mm	37	K_L
F021	48	111 ±1	111 ±1	0 ±2	0 ±.10	None	0	K_L
F014	81	112 ±11	34 ±1	78 ±11	.70 ±.03	Rec-1.3μ	0	K_L
2004	109	114 ±11	42 ±1	72 ±11	.63 ±.03	P-343μ	15.5	K_L
6200	59	114 ±11	105 ±10	9 ±15	.08 ±.09	None	0	K_L
F010	47	115 ±12	69 ±1	46 ±12	.41 ±.04	P-138μ Rec-6.9μ	22.8	K_L
6262	160	115 ±11	38 ±1	77 ±11	.67 ±.03	None	0	K_L
7117	48	115 ±12	88 ±1	27 ±12	.23 ±.07	Rec-2μ P-208μ	13.6	K_L
5001	75	116 ±12	116 ±15	0 ±19	0 ±.10	Rec-5.3μ	8	Out
7200	58	116 ±12	78 ±8	38 ±14	.33 ±.06	Rec-1μ	0	Out
6189	142	120 ±12	25 ±1	95 ±12	.79 ±.02	P-274μ P-45μ Rec-1.3μ	24.8	K_L
6136b	C.E.	120 ±12	-	-	-	P-186μ Rec-1μ	13.3	-
6057	97	121 ±12	74 ±1	47 ±12	.39 ±.05	Rec-2.6μ	4	K_L
F123	43	122 ±13	43 ±1	79 ±13	.65 ±.03	Rec-2.9μ P-25μ	13.5	K_L
1154	124	122 ±12	51 ±1	71 ±12	.58 ±.03	P-760μ Rec-2.8μ	24	K_L
1231	41	124 ±13	124 ±13	0 ±18	0 ±.10	Rec-1.6μ	2	Out

Code	θ Deg	T_i (Mev)	T_f (Mev)	T	T/T	Prongs Excl. K	Visible Energy Excl. K (Mev)	Decay Mode
3019	13	127 ±13	106 ±1	20 ±13	.16 ±.08	P-53u	10.4	K_L
6169	27	127 ±13	104 ±10	23 ±18	.18 ±.08	None	0	Out
7036	100	127 ±13	127 ±13	0 ±18	0 ±.10	Rec-1u	0	Out
F081	C. E.	177 ±14	-	-	-	Electron P-82u	11.2	-
1135	C.E.	138 ±13	-	-	-	Rec-7u P-400u	32.8	-
6088	101	128 ±14	56 ±1	72 ±13	.56 ±.04	P-4.9mm	43	K_L
F080	49	129 ±13	105 ±1	26 ±13	.19 ±.08	Rec-4u	6	K_L
6163	75	129 ±13	85 ±1	44 ±13	.34 ±.06	Rec-2u	3	K_L
F174	80	129 ±14	65 ±1	64 ±14	.50 ±.04	P-125 u Rec-1u	12.1	K_L
6189	74	130 ±13	94 ±1	36 ±13	.28 ±.07	P-167u	129	K_L
6009	169	131 ±14	41 ±1	90 ±14	.69 ±.03	P-8.4mm Rec-1u	55	K_L
6186	128	132 ±14	73 ±1	59 ±14	.45 ±.05	P-335u P-90u ec-2.6u	30.8	K_L
1042	C.E.	132 ±14	-	-	-	P-800u P-5.5u P-400u P-8.5u P-6.3mm	84.6	-
F111	43	134 ±13	99 ±10	35 ±16	.09 ±.09	Rec-1u	0	Out
7053	53	134 ±14	120 ±12	14 ±18	.09 ±.09	Rec-3u P-54u	14.9	Out
7122	103	134 ±14	74 ±1	46 ±14	.34 ±.05	Rec-1u Rec-1u	0	K_L
R014	64	134 ±14	113 ±12	21 ±19	.16 ±.08	Rec-5.2u P-23.5u	17.4	Out
5128	C.E.	134 ±14	-	-	-	P-373u P-1.1mm p-885u	60	-

Code	θ Deg	T_i (Mev)	T_f (Mev)	ΔT	$\Delta T/T$	Prongs Excl. K	Visible Energy Excl. K (Mev)	Decay Mode
F059	143	135 ±14	124 ±12	11 ±19	.08 ±.09	None	0	Out
6123	122	135 ±14	36 ±1	99 ±14	.73 ±.02	P-71u	10.9	K_L
7151	59	135 ±14	90 ±9	45 ±17	.33 ±.06	P-1.9mm	32	Out
F282	118	135 ±14	26 ±1	109 ±14	.81 ±.02	Rec-1μ P-13mm P-388μ	85	K_L
W018	C.E.	136 ±13	-	-	-	Rec-1μ P-3.2mm	44	-
1130	158	137 ±14	23 ±1	114 ±14	.83 ±.01	P-1.2mm P-665μ P-7.5mm	96	K_L
1206	49	138 ±14	118 ±1	20 ±14	.15 ±.09	Rec-1μ	0	K_L
1109	44	139 ±10	134 ±10	5 ±14	.04 ±.10	P-255μ	14.4	Out
1049	66	140 ±15	112 ±1	28 ±15	.20 ±.08	P-78μ P-32.8μ P-5.3μ	29	K_L
5034	23	140 ±15	134 ±1	6 ±15	.04 ±.10	P-348μ	15.6	K_L
7074	C.E.	140 ±15	-	-	-	Rec-1.8μ P-115μ	11.9	-
F087	35	142 ±14	106 ±1	36 ±14	.25 ±.08	None	0	K_L
1271	112	142 ±15	60 ±1	82 ±15	.58 ±.04	P-13.3mm	70	K_L
2033	97	142 ±15	60 ±1	82 ±15	.58 ±.04	P-64μ P-277μ	25.3	K_L
6008	114	145 ±12	94 ±10	51 ±16	.35 ±.06	Rec-1μ	0	Out
2014	99	146 ±16	29 ±1	117 ±16	.80 ±.02	P-7.4mm P-22μ	61.4	τ
F066	116	147 ±12	82 ±8	65 ±14	.44 ±.05	None	0	K_L
1036	14	148 ±16	73 ±1	75 ±16	.51 ±.04	None	0	K_L
2166	47	148 ±16	65 ±1	83 ±16	.56 ±.04	Rec-1μ	0	K_L

Code	θ Deg	T_i (Mev)	T_f (Mev)	ΔT	$\Delta T/T$	Prongs Excl. K	Visible Energy Excl. K (Mev)	Decay Mode
F146	C.E.	148 ±16	-	-	-	Electron P-53 μ P-7.4mm	62.4	-
6059	132	149 ±13	42 ±1	107 ±13	.72 ±.03	P-32 mm	110	τ
W041	73	149 ±20	95 ±10	54 ±22	.36 ±.06	P-29μ P-25.1μ Rec-1μ	19	Out
6108	100	150 ±16	56 ±1	94 ±16	.63 ±.03	Rec-2.3μ α-975μ P-11μ	71	K_L
F239	64	150 ±16	98 ±1	52 ±16	.35 ±.06	P-10.8mm	63	K_L
5091	C.E.	150 ±16	-	-	-	P-4.3mm	40	-
1038	82	151 ±16	46 ±1	105 ±16	.70 ±.03	P-33.3mm	112	$K_{\mu 3}$
6025	22	152 ±16	70 ±1	82 ±16	.54 ±.04	P-147 μ P-467μ P-123μ	41.6	τ'
5156	104	152 ±17	103 ±10	49 ±20	.32 ±.07	Rec-1μ	0	K_L
1102	105	153 ±17	50 ±1	103 ±17	.67 ±.03	P-169μ P-970μ	34.7	K_L
6010	79	154 ±11	102 ±10	52 ±15	.34 ±.07	Rec-2.3μ	3	K_L
J002	61	154 ±15	82 ±1	73 ±15	.47 ±.05	P-442μ	16.8	K_L
5183	77	154 ±17	54 ±1	100 ±17	.65 ±.08	P-26.2mm	32	K_L
2124	C.E.	155 ±17	-	-	-	None	0	-
5023	36	155 ±16	93 ±9	62 ±18	.40 ±.06	P-29μ P-49μ	19.4	Out
1004	84	156 ±17	93 ±1	63 ±17	.40 ±.06	Rec-1μ	0	K_L
1118	C.E.	156 ±16	-	-	-	Rec-1μ P-89μ	11.4	-
F083	58	158 ±18	134 ±14	24 ±23	.15 ±.09	Rec-1.3μ	0	Out
7110	10	158 ±17	140 ±15	18 ±23	.11 ±10	Rec-1μ	0	Out
5123	96	158 ±18	92 ±9	66 ±20	.42 ±.06	P-3.7mm	38	K_L

Code	θ Deg	T_i (Mev)	T_f (Mev)	ΔT	$\Delta T/T$	Prongs Excl. K	Visible Energy Excl. K (Mev)	Decay Mode
6007	104	160 ±18	123 ±12	37 ±22	.23 ±.08	P-8.7mm	56	Out
5118	171	162 ±18	52 ±5	110 ±19	.68 ±.03	P-21.6mm	90	Out
1347	49	163 ±18	89 ±1	74 ±18	.45 ±.05	P-5.1mm Rec-1μ	44	K_L
L028	111	164 ±19	44 ±1	120 ±19	.73 ±.02	None	0	K_L
6116	90	165 ±19	69 ±1	96 ±19	.58 ±.04	Rec-2μ P-7mm P-3.4mm	90	K_L
1370	C.E.	165 ±19	-	-	-	P-396μ Rec-1.6μ	16	-
1150	C.E.	165 ±19	-	-	-	P-633μ	18.7	-
F074	164	166 ±15	57 ±1	109 ±15	.66 ±.05	P-13mm-	69	K_L
W091	54	166 ±19	81 ±1	85 ±19	.51 ±.04	P-13 ±3mm	69	K_L
1178	69	167 ±19	56 ±1	111 ±19	.67 ±.03	Rec-1μ	0	K_L
W030	C.E.	167 ±14	-	-	-	α-29.8μ α-41.8μ α-4mm	100	-
6012	C.E.	167 ±14	-	-	-	None	0	-
7199	118	168 ±19	71 ±1	97 ±19	.58 ±.04	P-4.6mm	42	K_L
F246	81	168 ±19	148 ±16	20 ±25	.12 ±.10	Rec-1μ	0	K_L
2105	C.E.	169 ±20	-	-	-	P-1.64mm P-2.85mm	61	-
6219	47	170 ±20	40 ±1	130 ±20	.77 ±.02	P-71μ P-470μ	28.2	τ'
5058	25	170 ±20	38 ±1	132 ±20	.78 ±.02	None	0	K_L
6109	C.E.	171 ±20	-	-	-	Rec-1.3μ P-7.3mm P-2.5mm	84	-

Code	θ Deg	T_i (Mev)	T_f (Mev)	Δ T	Δ T/T	Prongs Excl. K	Visible Energy Excl. K (Mev)	Decay Mode
2071	42	176 ±20	176 ±20	0 ±30	0 ±.12	None	0	Out
1359	28	177 ±20	52 ±1	125 ±20	.71 ±.03	P-670μ P-278μ P-104μ	45.7	K_L
2190	53	177 ±20	132 ±14	45 ±25	.25 ±.08	Rec-2μ	3	Out
W089	84	177 ±16	96 ±10	81 ±18	.46 ±.05	P-650μ	19	Out
5182	78	179 ±19	69 ±1	110 ±19	.62 ±.03	Rec-5.3μ P-13.4mm P-555μ	96	K_L
7129	C.E.	179 ±21	-	-	-	Rec-2μ P-480μ	20	-
2178	120	180 ±21	57 ±1	123 ±21	.68 ±.03	P-484μ P-350μ Rec-1μ	32.8	K_L
5024	53	182 ±22	116 ±12	66 ±25	.36 ±.06	P-594μ	18.3	Out
1110	107	183 ±20	92 ±9	91 ±22	.50 ±.05	Rec-3μ	4.5	Out
F019	32	183 ±13	143 ±15	40 ±20	.22 ±.06	P-5μ P-4μ	7.5	Out
6126a	21	184 ±22	159 ±20	25 ±29	.14 ±.10	Rec-10.7μ	9	-
5105	129	185 ±22	79 ±1	106 ±22	.57 ±.04	P-312μ P-177μ	28.3	K_L
6075	138	186 ±22	45 ±1	141 ±22	.76 ±.02	P-38μ P-727μ Rec-2.6μ	28.7	K_L
5199	29	187 ±22	160 ±18	27 ±28	.14 ±.10	None	0	Out
6235	C.E.	187 ±22	-	-	-	P-285μ P-678μ Rec-1μ	34	-
7059	55	188 ±23	177 ±20	11 ±30	.06 ±10	Rec-1μ	0	K_L
5237	46	188 ±23	137 ±14	51 ±27	.27 ±.07	Rec-1μ	0	Out
1075	106	192 ±15	98 ±9	94 ±18	.49 ±.05	None	0	Out

Code	θ Deg	T_i (Mev)	T_f (Mev)	ΔT	$\Delta T/T$	Prongs Excl. K	Visible Energy Excl. K (Mev)	Decay Mode
5240	108	194 ±24	79 ±1	115 ±24	.59 ±.04	P-156μ Rec-2μ	15.7	K_L
2082	126	205 ±26	99 ±10	106 ±28	.52 ±.05	P-293μ Rec-1μ	14.9	Out
6153	3	205 ±26	175 ±1	30 ±26	.15 ±.10	None	0	K_L
6061	C.E.	207 ±15	-	-	-	Electron Rec-0.8μ P-6.5mm	49	-
W022	132	210 ±20	69 ±6	141 ±21	.67 ±.05	Rec-1μ P-[illegible].3mm	45	Out
7113	108	212 ±20	15 ±1	197 ±20	.93 ±.01	P-74.4mm Rec-2.4μ	177	K_L
5177	44	235 ±40	144 ±15	91 ±43	.39 ±.06	None	0	Out

probability that no interaction occurs is exp $(-VA/V_n)$. Therefore, the total cross section for inelastic collisions is

$$\sigma = 2\pi \int_0^{R+r_1} \left[1 - \exp(-VA/V_n) \right] b\, db \qquad (D\text{-}4)$$

where r_1 is the interaction radius defined by

$$\bar{\sigma} = \pi r_1^2 \qquad (D\text{-}5)$$

Equation E-4 may be re-expressed by use of the geometric cross section $\sigma_0 = \pi R^2$ as follows

$$\frac{\sigma}{\sigma_0} = 2 \int_0^{R+r_1} \left[1 - \exp(-VA/V_n) \right] \frac{b}{R} \frac{db}{R} \qquad (D\text{-}6)$$

Since $r_1 << R$, V can be approximated by

$$V = 2\bar{\sigma}\sqrt{R^2 + b^2} \qquad (D\text{-}7)$$

Then

$$\exp(-VA/V_n) = \exp\left(-2\sqrt{R^2+b^2}/\ell_c\right) \qquad (D\text{-}8)$$

where $2\sqrt{R^2 - b^2}$ represents the thickness of nuclear matter traversed by the K, and

$$\ell_c = \frac{V_n}{A\bar{\sigma}} = \frac{4}{3}\pi r_0^3/\bar{\sigma} \qquad (D\text{-}9)$$

represents the collision mean free path in nuclear matter.

Also equation E-6 becomes

$$\frac{\sigma}{\sigma_0} = 2\int_0^R \left[1 - \exp\left(-2\sqrt{R^2+b^2}/\ell_c\right)\right] \frac{b}{R}\frac{db}{R} = 1 - t\left(\frac{\ell_c}{R}\right) \qquad (D\text{-}10)$$

where

$$t\left(\frac{\ell_c}{R}\right) = \frac{\ell_c^2}{2R^2}\left[1 - \exp(-2R/\ell_c) - 2R/\ell_c \exp(-2R/\ell_c)\right] \qquad (D\text{-}11)$$

Physically, t represents the average transparency of the nucleus, i.e.,

the probability of traversal without interaction averaged over all possible paths through the nucleus. Figure 15 shows a plot of Equation E-10. Only approximated curves for the heavy and light element groups of emulsion are shown.

The calculation of the cross section per nucleon from the mean free path for inelastic collision in emulsion was as follows:

An approximate value of ℓ_c was estimated using an average emulsion nucleus. Using this value of ℓ_c the values of $\frac{\ell_c}{R}$ were evaluated for each nucleus in emulsion (excluding hydrogen). Then using Figure 15 these were converted to σ/σ_0 in each case. These were then combined to give the mean free path as follows:

$$\lambda = \frac{1}{\sum_i N_i \sigma_i} = \frac{1}{\sum_i \frac{\rho_i}{A_i} L \left(\frac{\sigma}{\sigma_0}\right)_i \sigma_{0i}} = \frac{1}{\sum_i \frac{\rho_i}{A_i} \frac{1}{3} \left(\frac{\sigma}{\sigma_0}\right)_i \pi r_0^2 L} \qquad \text{(D-12)}$$

where L is Avagadro's number and $\left(\frac{\sigma}{\sigma_0}\right)_i$ are the graphically determined values for each nucleus. The summation is taken over all the elements of emulsion excluding hydrogen. On completion of this evaluation, a series of about ten values of the parameter ℓ_c were chosen in the immediate neighborhood of interest and the process repeated for each to obtain the mean free path in emulsion represented by each. Each ℓ_c gave a corresponding $\bar{\sigma}$ by

$$\bar{\sigma} = \tfrac{4}{3} \pi r_0^3 / \ell_c \qquad \text{(D-13)}$$

The calculation was done for various values of r_0 and the resulting information was plotted in Figure 16.

The allowance for Coulomb repulsion which reduces the measured

Figure 15

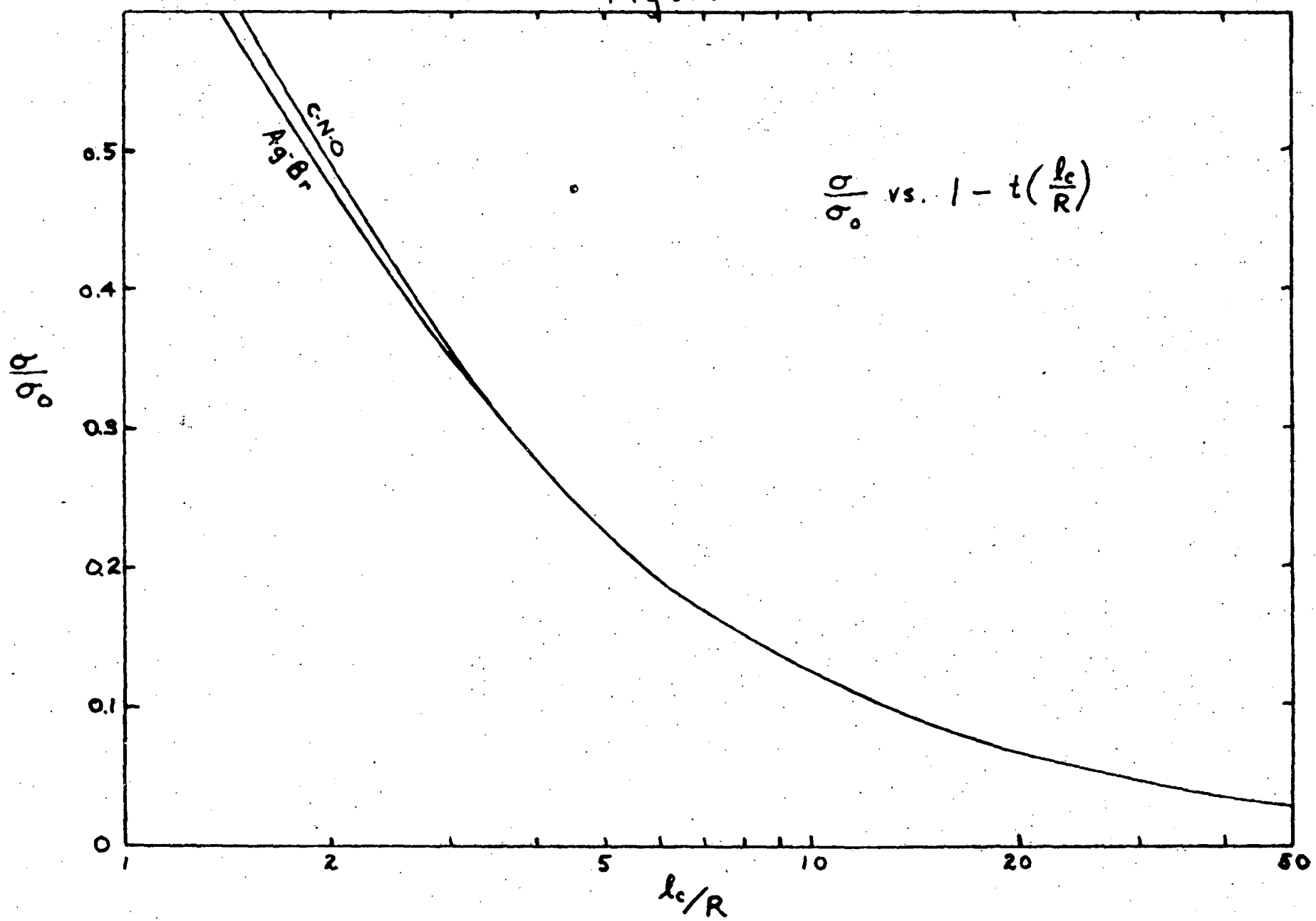
C-N-O
Ag-Br
$\frac{\sigma}{\sigma_0}$ vs. $1 - t\left(\frac{l_c}{R}\right)$
$\frac{\sigma}{\sigma_0}$
0.5
0.4
0.3
0.2
0.1
0
1
2
5
10
20
50
l_c/R

Figure 16

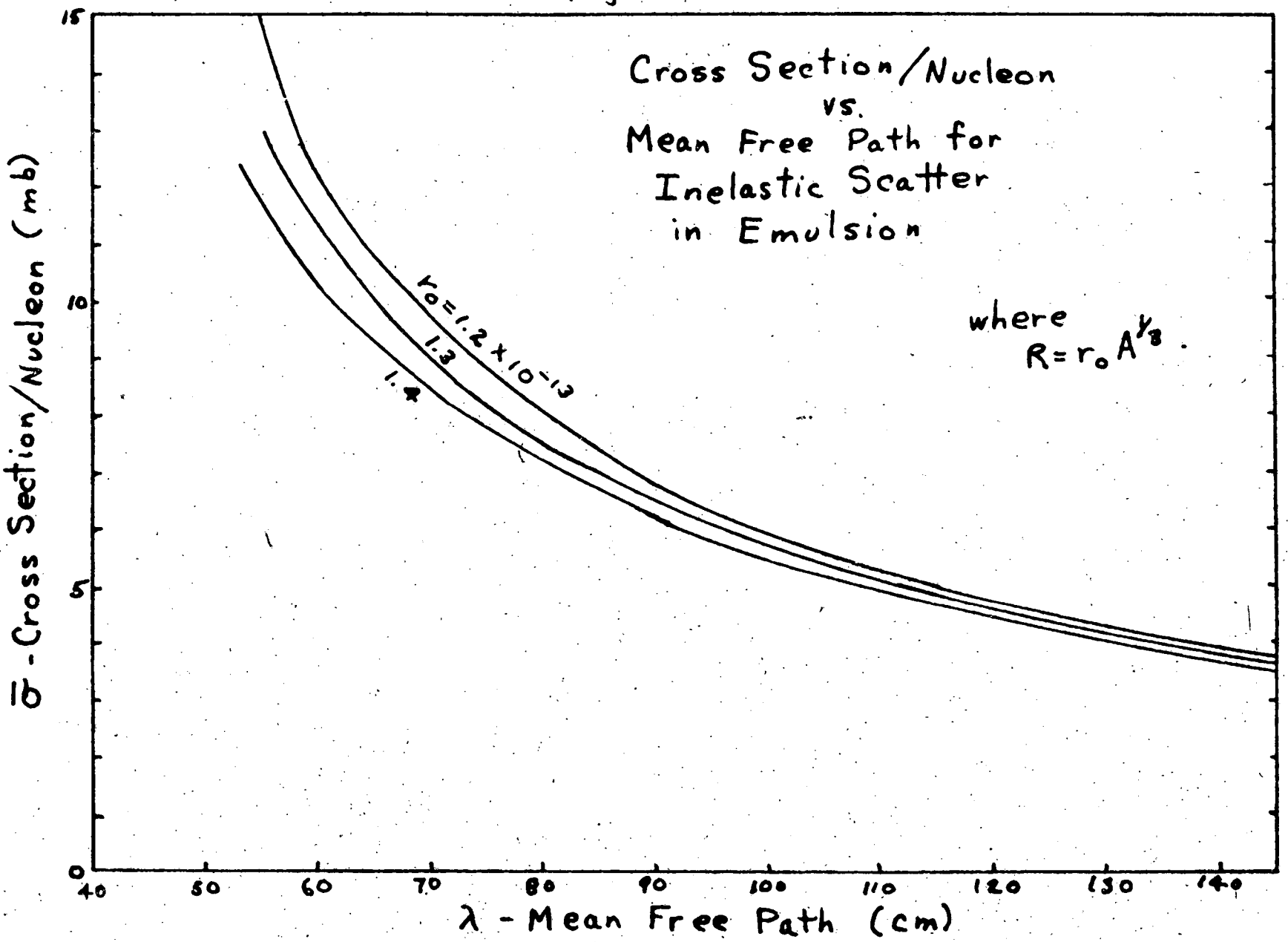
Cross Section/Nucleon
vs.
Mean Free Path for
Inelastic Scatter
in Emulsion
where
$R = r_0 A^{1/3}$.
$r_0 = 1.2 \times 10^{-13}$
1.3
1.4
$\bar{\sigma}$ - Cross Section/Nucleon (mb)
λ - Mean Free Path (cm)
0
5
10
15
40
50
60
70
80
90
100
110
120
130
140

cross section for each nucleus was made using the approximation given by Blatt and Weisskopf[58]

$$\sigma_{i_{obs.}} = \sigma_i \left[1 - \frac{(Z_i - 1)\, e^2}{(R_i + \lambda\!\!\!^{-})\, T} \right] \equiv \sigma_i\, f(R_i, Z_i, T) \qquad \text{(D-14)}$$

where R_i is the nuclear radius of the ith element, Z_i is its charge, $\lambda\!\!\!^{-}$ is the deBroglie wavelength of the incident K meson, and T is its kinetic energy. The factor f was evaluated for each emulsion nucleus for each of the five energy intervals of interest. Then for each energy interval equation E-12 was re-evaluated for

$$\lambda_T = \frac{1}{\sum_i N_i \sigma_i f(R_i, Z_i, T)} \qquad \text{(D-15)}$$

The results are shown in Figure 17 for $r_o = 1.2 \times 10^{-13}$ cm.

Figure 17

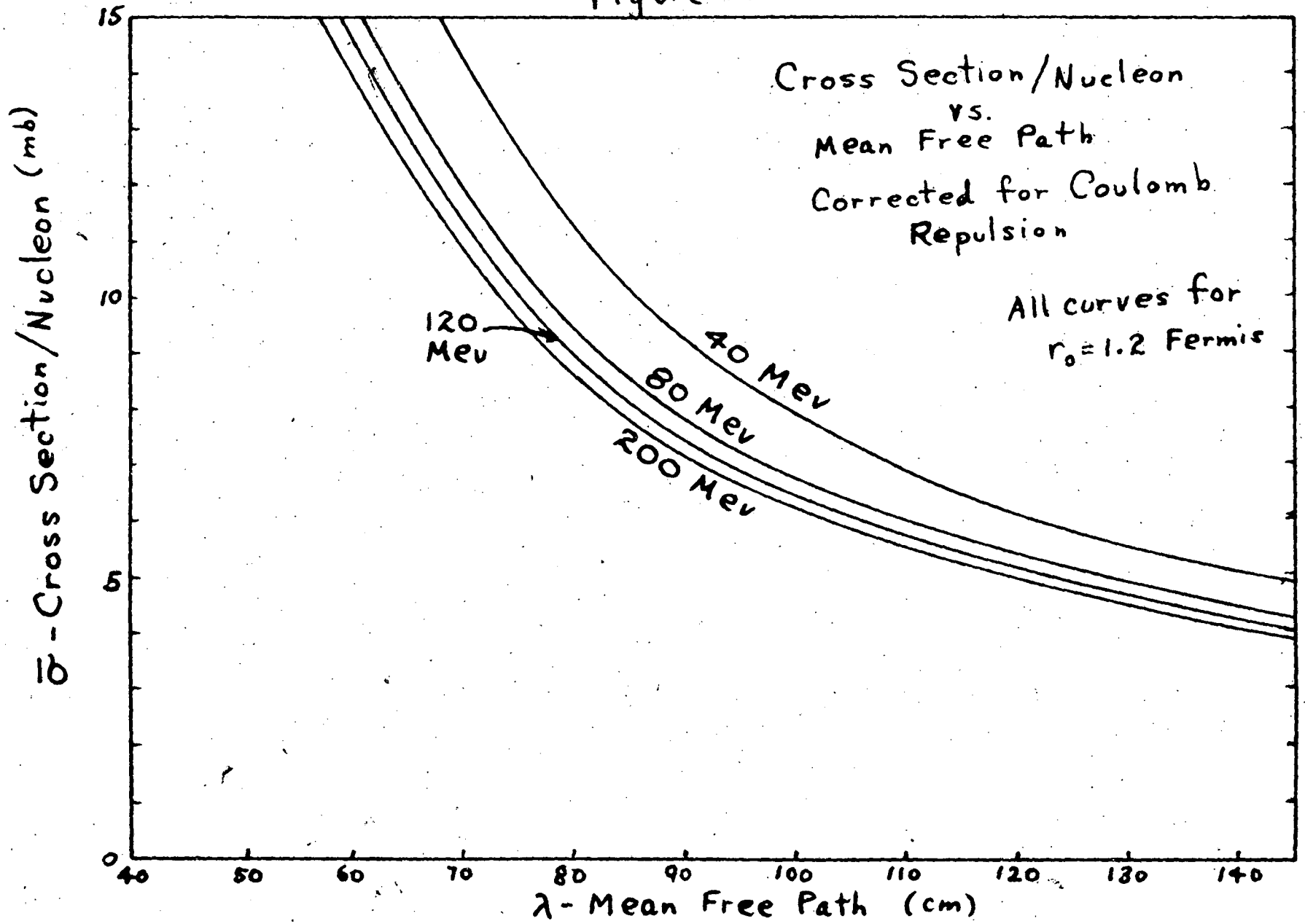
Cross Section/Nucleon
vs.
Mean Free Path
Corrected for Coulomb
Repulsion
All curves for
$r_0 = 1.2$ Fermis
40 Mev
80 Mev
120 Mev
200 Mev
$\bar{\sigma}$ - Cross Section/Nucleon (mb)
λ - Mean Free Path (cm)
0
5
10
15
40
50
60
70
80
90
100
110
120
130
140

APPENDIX E

Related work:

Between the time of publication of the work done in Phase I of this experiment (Pisa Conference, June 1955, and Physical Review, March 1956) and completion of Phase II, a considerable amount of work has been done along the same lines by other laboratories. For convenient reference, here are given abstracts of some of the publications and preprints known to us at the present time. Many of the conclusions are similar to those given in this present work.

Interactions of K^+ Mesons with Hydrogen Nuclei at 50 to 110 Mev.

N. N. Biswas, L. Ceccarelli-Fabbrichesi, M. Ceccarelli, M. Cresti, K. Gottstein, N. C. Varshneya and P. Waloschek, of Gottingen.

Il Nuovo Cimento, Vol. III, N. 6, p. 1481 (June 1956)

In this work 162 meters of K^+ meson track were followed in the energy interval 0 to 110 Mev. Twelve K-hydrogen events were found. The resulting cross section from this data was 23 $\pm$ 7 mb.

Nuclear Scattering of K^+ Mesons in the Energy Region of 80 Mev.

N. N. Biswas, L. Ceccarelli-Fabbrichesi, M. Ceccarelli, K. Gottstein, N. C. Varshneya and P. Waloschek, of Gottingen.

Il Nuovo Cimento, Vol. V, N. 1, p. 123 (January 1957)

The scattering of K^+ mesons by nuclei of photoemulsion was investigated. In this work 105 meters of track were followed in the 60 to 100 Mev region.

The angular distribution of the elastic scatterings was compared with the curves calculated by Costa and Patergnani for the

optical model of the nucleus. The data definitely favored a repulsive nuclear potential of about 12 Mev.

The inelastic scattering data was compared with the results of a calculation performed with the Monte Carlo method, for a Fermi gas nuclear model. Best agreement was found with experimental data by assuming that the cross section was isotropic in the center of mass system up to an energy of 40 Mev and then rises backward at higher energies and has the form $(2.5 - 1.5 \cos \theta)$. The energy loss behaviour agreed best with the assumption that there is a repulsive nuclear potential of 20 Mev.

A collection was presented of K^+-hydrogen scatterings found in nuclear emulsion at various laboratories. Data on 27 events with center of mass angle greater than 16° is given. The total cross section (for energies less than 150 Mev) was found to be 14 ± 3 mb. The angular distribution of the events agreed best with a repulsive nuclear potential and predominant S wave scattering. The cross section was observed to be not strongly energy dependent.

K^+ Meson Interaction with Nucleons and Nuclei.

G. Cocconi, G. Puppi, G. Quareni, and A. Stranghellini, of Bologna.

Il Nuovo Cimento, Vol. V, N. 1, p. 172 (January 1957).

The results obtained in several laboratories on the nuclear interaction of the K^+ mesons of energy between 40 and 150 Mev were analyzed. The main results were the following: (1) The total cross section for the process $K^+ + P$ (isotopic spin state $T = 1$) is 14 ± 3 mb. The corresponding differential cross section may be described essentially

by constructive interference between S wave and Coulomb scattering. (2) The isotopic spin state T = 0 is not negligible compared to T = 1. P wave should be important in the T = 0 state. (3) To explain the K^+ meson interaction with nuclei, a nuclear repulsive potential V = 10 Mev should be added to the Coulomb potential. With these assumptions it is possible to describe: (a) the elastic scattering in terms of the optical model. (b) The inelastic scattering, by considering the interaction due to single collisions of the K^+ mesons with the nucleons. (4) The K^+ nucleon interaction in the T = 1 state may be described by a central potential equivalent to a hard-core of radius $a = 0.8(\hbar/m_K c)$.

Interactions of K^+ Mesons with Emulsion Nuclei between 40 and 160 Mev.

M. Baldo-Ceolin, M. Cresti, N. Dallaporta, M. Grilli, L. Guerriero, M. Merlin, G. A. Salandin and G. Zago, of Padova.

Il Nuovo Cimento, Vol. V, N. 2, p. 402 (February 1957)

In this work 110 meters of K^+ track were followed in the energy interval 40 to 160 Mev. The events observed were 5 K-hydrogen scatters, 91 inelastic scatters, 10 charge exchanges and 56 decays in flight. Events were divided into two energy intervals 40-90 Mev and 90-160 Mev.

The total elastic cross section for angles greater than 20° was measured. The number of scatterings between 7° and 13° on 10 meters of track was determined. These data were compared with the calculations of Costa and Patergnani and it was concluded that there exists a repulsive potential of about 15 Mev.

Montecarlo calculations to predict the behaviour of energy

losses assuming the experimental angular distribution indicated that a best fit could be obtained by using a nuclear potential plus coulomb potential of 20 Mev.

It was found that the inelastic scattering of K^+ with nucleons in nuclear matter was characterized by: (1) an apparent total cross section much lower (about 4 mb) than the K-P cross section; (2) this cross section appears to increase with energy; (3) the differential cross section seems to be strongly peaked backwards in the center of mass; (4) the cross section for charge exchange events is much smaller than the scattering cross sections. These features were explained by assuming that the Pauli principle is important and that it cuts out most of the forward scattering in nuclear matter, thus also reducing the total cross section.

It was concluded that the data shows that there is an important contribution in the T = 1 state, as an S-wave, in the low energy interval, whereas at higher energies the presence of a P-wave, possibly, of the T = 0 state, seems probable.

The Interactions of Positive K-Mesons with Nuclei in Photographic Emulsion at Energies between 0-130 Mev.

B. Bhowmik, D. Evans, S. Nilsson, D. J. Prowse, F. Anderson, D. Keefe, A. Kernan, and J. Losty, of Bristol and Dublin U. C.

Privately circulated preprint.

In following 148 meters of K^+ track 109 inelastic interactions with emulsion nuclei and 3 K-hydrogen scatters were found. The total elastic cross section for angles greater than 20° was determined.

Accepting the K-nucleus potential as repulsive, the work of Costa and Patergnani was used to evaluate the nuclear potential in three energy regions: 40-70 Mev, V = +12 Mev; 70-100 Mev, V = +18 Mev; and 100-130 Mev, V = +20 Mev.

The variation of cross section with energy for the inelastic events was found to be consistent with isotropy if the Pauli exclusion principle was taken into account and the best fit for the experimental points was obtained for a repulsive well depth of 20 Mev. The average K-nucleon cross section within nuclear matter for meson energies between 60 and 130 Mev was found to be 5.5 mb; allowing for the events forbidden by the exclusion principle this implied a cross section of 8 $\pm$ 1 mb on a free nucleon. If σ_P = 14 $\pm$ 3 mb, it followed that σ_N = 6 $\pm$ 3 mb.

The ratio of charge exchange events to non-charge exchange events was 0.20 $\pm$ 0.07 -- the value expected in the limit of a vanishingly small interaction in the T = 0 state, leaving only interaction in the T = 1 state.

The inelastic events were analyzed on the basis of the statistical model of Goldberger and an attempt was also made to obtain for the experimental data the angular distribution in the center of mass system of the K nucleon. On any reasonable assumption this appeared to be peaked backwards. The data also demanded a repulsive potential of 20 Mev.

BIBLIOGRAPHY

1. Rochester and Butler, Nature 160, 855 (1947).

2. Brown, Camerini, Fowler, Muirhead, Powell and Ritson, Nature 163, 82 (1949).

3. Amaldi, Amderson, Blackett, Fretter, LePrince-Ringuet, Peters, Powell, Rochester, Rossi and Thompson, Nature 173, 123 (1954); Physics Today 6, No. 12, 24 (1953).

4. A. M. Shapiro, Rev. of Mod. Phys., Vol. 28, No. 2, 164 (1956).

5. Ekspong and Goldhaber, Phys. Rev. 102, 1187 (1956).
Williams, Haskin, Koshiba, and Schein, Phys. Rev. 100, 1547(1955).
Van Lint and Trilling, Phys. Rev. 92, 1089 (1953).

6. Dalitz, Phil. Mag. 44, 1068 (1953); Phys. Rev. 94, 1046 (1954).
Haddock, "Analysis of Bevatron Taus," Thesis, UCRL-3580 (Nov. 1956).

7. Lee and Yang, "Is Parity Conserved in Weak Interactions?", Preprint, submitted to Phys. Rev.
Wu, Ambler, Hayward, Hoppes and Hudson, "An Experimental Test of Parity Conservation in Beta Decay," preprint, submitted to Phys. Rev.

8. Peterson, "The Masses of Identified Positive Heavy Mesons," UCRL-3368 (April 1956).

9. Webb, Chupp, Goldhaber, and Goldhaber, Phys. Rev. 101, 1212 (1956).

10. Iloff, "Interactions and Lifetimes of K mesons," Thesis, UCRL-3605 (Nov. 1956).

11. Alvarez, Crawford, Good, and Stevenson, Phys. Rev. 101, 496 (1956).
Hoang, Kaplon, and Yekutieli, "Lifetimes of τ, $K_{\mu 3}$, and K_e Decay Modes," preprint, submitted to Phys. Rev.

12. A. Pais, Phys. Rev. 86, 663 (1952).

13. M. Gell-Mann and A. Pais, Proceedings of the Glasgow Conference on Nuclear and Meson Physics, Pergamon Press, London (1955).

Similar ideas have been presented by

T. Nakano and K. Nishijima, Prog. Theo. Phys. 10, 581 (1953).

R. G. Sachs, Phys. Rev. 99, 1573 (1955).

M. Goldhaber, Phys. Rev. 92, 1297 (1953); 101, 433 (1956).

14. Chupp, Goldhaber, Goldhaber, and Webb, Proc. of 1955 Pisa Conf., Suppl. to Nuovo Cimento, 1956.

Alvarez, Bradner, Falk-Vairant, Gow, Rosenfeld, Solomitz, and Tripp, "K⁻ Interactions in Hydrogen," UCRL-3583 (Nov. 1956).

15. Chupp, Goldhaber, Goldhaber, Iloff, Lannutti, Pevsner, and Ritson, Proc. of 1955 Pisa Conf., Suppl. to Nuovo Cimento, 1956.

16. Lannutti, Chupp, Goldhaber, Goldhaber, Helmy, Iloff, Pevsner, and Ritson, Phys. Rev. 101, 1617 (1956).

17. Biswas, Fabbrichesi, Ceccarelli, Gottstein, Varshnoya and Waloschek, Nuovo Cimento 5, 123 (1957).

18. Ceolin, Cresti, Dallaporta, Grilli, Guerriero, Merlin, Salandin, and Zago, Nuovo Cimento 5, 402 (1957).

19. Bhowmik, D. Evans, Nilsson, Prowse, Anderson, Keefe, Kernan, and Losty, "The Interactions of Positive K-Mesons with Nuclei in Photographic Emulsion at Energies between 0-130 Mev," Preprint.

20. Kerth, Stork, Haddock, and Whitehead, Phys. Rev. 99, 641(A)(1955).

21. Rosenfeld, "How to Devil-up Plates," privately circulated.

22. Goldhaber, Goldsack, and Lannutti, "Method for Alignment of Stripped Nuclear Emulsions," UCRL-2928 (Mar. 1955).

23. Goldschmidt-Clermont, Annual Review of Nuclear Science, Vol. 3, p. 141 (1953).
G. Ekspong, Arkiv För Fysik 9, Nr. 5, 49 (1954).

24. Opacity is the percentage blackness of a track and was used in those regions where grain count was not reliable, i.e., above three times minimum where saturation becomes important. It is the natural extension of grain counting and may be done with comparable ease. Best results are obtained using a magnification of 25x100 and a reticle with 100 divisions.

25. D. H. Stork, "Notes on the 60° Separated K Beams," Sept. 26, 1956 privately circulated. Re-printed as UCRL Bev. 186.

26. Eng. Note 4902-02 MT-2, Oct. 3, 1955.

27. L. Stevenson, private communication.

28. A. Pais and R. Serber, Phys. Rev. 99, 1551 (1955).

29. The tables of Baker and Curtis, "Tables of K Meson Scattering by Protons," UCRL-3274, greatly facilitated this work.

30. Chupp, Goldhaber, Goldhaber, Johnson, and Lannutti, Phys. Rev. 99, 1042 (1955).

31. Communications of the Bristol, Dublin U.C., Gottingen and Padova groups, Turin Conference, Sept. 1956.
Biswas, Ceccarelli-Fabbrichesi, Ceccarelli, Cresti, Gottstein, Varshneya, and Waloschek, Nuovo Cimento 1, 137 (1957).
Sechi-Zorn and Zorn, private communication.

32. Meyer, Perl, and Glasser, Preprint, submitted to Phys. Rev.

33. Kerth, Kycia, and Van Rossum, private communication.

34. Based on four times as much data in this energy region, B. Sechi-Zorn and G. T. Zorn (Private communication) have observed the same increase and obtain the same mean free path. It is interesting to note that the threshold for π production by K's on free protons is about 225 Mev.

35. M. Goldberger, Phys. Rev. 74, 1269 (1948).

36. B. Rossi, High Energy Particles, Prentice-Hall, Inc.(1952), p. 359.

37. R. M. Sternheimer, "Effect of the Exclusion Principle on the Interaction of K Mesons with Nuclei," preprint, submitted to the Phys. Rev.

38. Proc. of the 6th Annual Rochester Conference, April 1956, Section VI-16.

39. Osborne, Phys. Rev. 102, 296 (1956).

40. Fournet Davis, Preprint, submitted to the Phys. Rev.

41. Costa and Patergnani, Nuovo Cimento 5, 448 (1957).

42. Francis and Watson, A. J. P. 21, 659 (1953).

43. L. I. Schiff, Quantum Mechanics, McGraw Hill Book Co., Inc., (1949) Sec. 20.

44. Hahn, Ravenhall, and Hofstadter, Phys. Rev. 101, 1131(1956).

45. Strauch and Titus, Phys. Rev. 103, 200 (1956).

46. Fernbach, Serber, and Taylor, Phys. Rev. 75, 1352 (1949).

47. See, e.g., Camerini, Lock, and Perkins, Progress in Cosmic Ray Physics, North Holland Publishing Company, Amsterdam (1952); Bernardini, Cortini, and Manfredini, Phys. Rev. 79, 952 (1950); Nora Page, Proc. Phys. Soc. A63, 250 (1950).

48. Range-energy tables of W. H. Barkas, October 30, 1956.

49. V. Weisskopf, Phys. Rev. 52, 295 (1937).

50. K. J. LeCouteur, Proc. Phys. Soc. A63, 259 (1950).

51. Bailey, "Angle and Energy Distributions of Charged Particles from the High Energy Nuclear Bombardment of Various Elements," Thesis, UCRL-3334, March 1956.

52. E. Segrè, Experimental Nuclear Physics, Vol. II, p. 173, John Wiley and Sons (1953).

53. L. I. Schiff, Quantum Mechanics, p. 111.

54. Bethe and de Hoffmann, Mesons and Fields, Vol. II, Row-Peterson (1955), p. 66.

55. Stapp, "Chew Theory Approach to the Scattering of Low Energy K^+ Particles by Nucleons," UCRL-3535.

56. T. F. Hoang, private communication.

57. Reynolds and Zucker, Phys. Rev. 96, 393 (1954).

58. Blatt and Weisskopf, Theoretical Nuclear Physics, John Wiley and Sons (1952), p. 350.